DnaA modulates the gene expression and morphology of the Lyme disease spirochete

Andrew C. Krusenstjerna[1], Nerina Jusufovic[1], Timothy C. Saylor[1], Brian Stevenson[1,2]

1. Department of Microbiology, Immunology, and Molecular Genetics, University of Kentucky College of Medicine, Lexington, Kentucky, USA
2. Department of Entomology, University of Kentucky, Lexington, Kentucky, USA

Address for correspondence:
Department of Microbiology, Immunology, and Molecular Genetics
University of Kentucky, College of Medicine
Lexington, Ky. 40536-0278
Email: brian.stevenson@uky.edu
Phone: 1-859-257-9358

ABSTRACT.

All bacteria encode a multifunctional DNA-binding protein, DnaA, which initiates chromosomal replication. Despite having the most complex, segmented bacterial genome, little is known about *Borrelia burgdorferi* DnaA and its role in maintaining the spirochete's physiology. In this work we utilized inducible CRISPR-interference and overexpression to modulate cellular levels of DnaA to better understand this essential protein. Dysregulation of DnaA, either up or down, increased or decreased cell lengths, respectively, while also significantly slowing replication rates. Using fluorescent microscopy, we found the DnaA CRISPRi mutants had increased numbers of chromosomes with irregular spacing patterns. DnaA-depleted spirochetes also exhibited a significant defect in helical morphology. RNA-seq of the conditional mutants showed significant changes in the levels of transcripts involved with flagellar synthesis, elongation, cell division, virulence, and other functions. These findings demonstrate that the DnaA plays a commanding role in maintaining borrelial growth dynamics and protein expression, which are essential for the survival of the Lyme disease spirochete.

IMPORTANCE.

Lyme disease is the most prevalent tick-borne infection in the Northern Hemisphere. *Borrelia burgdorferi*, the causative spirochete bacteria, has been maintained in nature for millennia in a consistent enzootic cycle between *Ixodes* ticks and various small vertebrate hosts. During the tick's blood meal, *B. burgdorferi* substantially increases its replication rate, alters its repertoire of outer surface proteins, and disseminates into the new vertebrate host. Across eubacteria, DnaA is the master regulatory protein that initiates chromosomal replication and acts as a transcription factor to regulate specific pathways. Here, we describe the roles that *B. burgdorferi* DnaA has on the physiology and gene expression of this medically important pathogen.

Introduction.

Replication plays a significant role in the enzootic lifecycle of *Borrelia burgdorferi*, the Lyme disease spirochete. An extracellular bacterial parasite, *B. burgdorferi* exclusively colonizes Ixodid ticks and assorted vertebrates (1, 2). Naïve tick larvae acquire the Lyme bacteria when they feed on an infected host. After this single blood meal, the larvae drop off, overwinter, and molt to their nymphal stage. During this time, *B. burgdorferi* persists within the midgut of the nutrient-deplete tick. Once the nymph emerges and takes its blood meal, the spirochetes obtain the requisite materials to replicate, divide, and disseminate from the tick to the new vertebrate host (3, 4).

The highly conserved AAA+ family protein DnaA initiates the replication of bacterial chromosomes (5-7). DnaA monomers recognize the *oriC* locus and cooperatively multimerize to form a helical structure. The DnaA filament promotes the separation of AT-rich DNA elements, which recruits helicase and replication machinery. DnaA not only initiates chromosomal replication but also binds elsewhere in the genome to regulate gene expression (8, 9). We recently found that *B. burgdorferi* DnaA directly regulates the *dnaX-ebfC* operon, which codes for the Tau (τ) subunit of DNA polymerase III holoenzyme, DnaX, and a regulatory nucleoid-associated protein, EbfC (10). These genes are highly expressed during periods of rapid spirochete replication (10-12). At the tick-vertebrate interface, we hypothesize that *B. burgdorferi* DnaA not only commits to its replication initiation function but coordinates the expression of genes needed for vertebrate infection (10, 13, 14).

Replication of the *B. burgdorferi* linear chromosome proceeds bidirectionally from the centrally-located *oriC* (15). Outside of this, little is known about borrelial DNA replication, its regulation, or coordination with other cellular processes. Many of the genes involved in those

pathways are essential, which has hampered their investigation. Historically, studying essential loci required the development or isolation of conditional mutants. The first studies into bacterial DnaA proteins utilized temperature-sensitive mutants (16). In the era of molecular genetics, many tools have been developed to produce conditional phenotypes more readily, such as inducible promoters. Overexpression has been a reliable means of elucidating a protein's function in *B. burgdorferi* and other bacteria (14, 17, 18). Recently, inducible CRISPR interference (CRISPRi) systems have been developed and added to the repertoire of tools for studying borrelial biology (19, 20). This work will describe the consequence of CRISPRi-mediated knockdown of the essential replication initiator protein DnaA in *B. burgdorferi*. Using this approach, coupled with overexpression, we observed profound consequences of DnaA-dysregulation on spirochete morphology, chromosome partitioning, and gene expression.

RESULTS.

Construction and validation of plasmids to dysregulate levels of DnaA in *B. burgdorferi*. DnaA is essential for initiating chromosomal replication, so deleting DnaA is lethal to bacteria. Thus, to gain insight into the impacts of DnaA on borrelial physiology, we produced IPTG-inducible constructs to reduce or elevate cellular levels of DnaA. Knockdown was carried out using the newly refined all-in-one CRISPR interference (CRISPRi) shuttle vector, which places the expression of both the sgRNA and a borrelial codon-optimized dCas9 gene under the control of the Lac repressor (20). We designed two CRISPRi constructs with sgRNAs targeting either the template (*dnaA*$_{T1}$) or non-template (*dnaA*$_{NT1}$) DNA strands directly 5' or within the *dnaA* gene (**Fig. 1A**). Overexpression was achieved using plasmid pACK121, which contains an inducible *dnaA* with an N-terminal 3xFLAG tag. All constructs were transformed into *B. burgdorferi* strain B31-e2, hereafter referred to as e2. The spirochetes tolerated each construct well, replicating at rates comparable to the parental strain without the inducer (**Fig. 1B**), with one exception. The *dnaA*$_{T1}$ CRISPRi strain replicated slightly slower than the others, although it reached the same final density. This may suggest leakiness of the hybrid *lac* promoter that controls the sgRNA and dCas9 gene (B. Murphy & W. Zückert, personal communication).

To assess the efficacy of these inducible constructs, spirochetes of each strain were grown to mid-exponential growth phase (3-5x10^7 cells/mL), then incubated overnight with 0.5 mM IPTG. The *dnaA*-targeting CRISPRi strains decreased the expression of DnaA, with the construct targeting the template strand, *dnaA*$_{T1}$, consistently yielding the most effective gene silencing (**Fig. 1C** and **D**). The potency of the *dnaA*$_{T1}$ construct likely explains the slowed spirochete growth seen in the absence of IPTG (**Fig. 1B**). Overexpression resulted in elevated quantities of DnaA protein and transcript (**Fig. 1C** and **D**). Neither the CRISPRi empty vector

(EV) nor the parental e2 control strains yielded changes in DnaA levels when IPTG was added, demonstrating that we could specifically and effectively alter cellular DnaA concentrations.

Proper DnaA expression is essential for borrelial growth. Given its essential nature for chromosomal replication, we first sought to evaluate the consequence of DnaA dysregulation on *B. burgdorferi* growth and cell division. To achieve this, all strains were grown to mid-exponential phase and passaged into fresh media with 0.5 mM of IPTG at a density of $1x10^5$ cells/mL. Bacterial numbers of each culture were counted every day for seven days to generate growth curves.

CRISPRi knockdown of DnaA levels substantially reduced the generation time and carrying capacity of *B. burgdorferi* (**Fig. 2A** and **B**). The severity of these phenotypes was consistent with the knockdown efficacy of the two constructs, with $dnaA_{NT1}$ cultures reaching a maximum density that was one log lower and $dnaA_{T1}$ cultures maxing out two logs lower than the controls. This suggests that reducing the cellular concentration of DnaA directly limits the number of division cycles, which is consistent with DnaA's role as the chromosomal replication initiator.

Overproducing DnaA slowed growth during the first four days post-inoculation (dpi), growing at a rate similar to the $dnaA_{T1}$ culture (**Fig. 2A** and **B,** early). After that time, however, cultures consistently resumed logarithmic growth, yielding generation times that were indistinguishable from the parental strain (**Fig. 2B**, late). We hypothesized this abrupt resumption of growth was due to mutations in the inducible *dnaA* plasmid that eliminated overexpression. To test this, we passaged spirochetes that had resumed growth into fresh media with IPTG to see if growth would still be perturbed. Consistent with our hypothesis, these "conditioned" bacteria immediately grew at rates that were similar to the control strain (**Fig. 2C**),

and induction of the 3xFLAG tagged DnaA did not occur (**Fig. 2D**). To further test our hypothesis, we extracted the DnaA overexpression plasmid from the *B. burgdorferi* cultures and transformed them into *E. coli*. We sequenced purified plasmids from two colonies derived from the same induced borrelial culture. Each clone had unique mutations within the *dnaA* ORF that truncated the full-length protein (**Fig. 2E**). Notably, both mutations resulted in the complete loss of domain IV, the DNA-binding domain of DnaA. Plasmid isolated from transformed *B. burgdorferi,* which had never been exposed to IPTG, had no mutations within the inducible *dnaA*. These escape mutants, taken with the growth dynamics, highlight the stressful nature of *dnaA* overexpression, which has consistently been observed in other bacterial organisms (21-23).

Unlike the overexpression strain, we never observed a resumption of growth in the induced *dnaA* CRISPRi strains. Furthermore, normal growth was attainable from knocked-down cultures after passaging spirochetes into fresh media without IPTG. These collective data demonstrate that precisely controlled levels of DnaA are required for optimal borrelial growth.

DnaA affects spirochete cell division/elongation. Chromosomal replication is intimately tied to cellular elongation and division (24-26). Having found that the conditional DnaA mutants had replication defects, we also sought to assess the impact of DnaA dysregulation on *B. burgdorferi* cell length. Over seven days, we imaged and measured spirochetes. In the parental e2 cultures, we observed a consistent pattern wherein median cell length peaked during early exponential phase, followed by a steady decrease, then stabilization once the cultures reached stationary phase (**Fig. 3A**, **3E,** and **3I**).

These findings sharply contrast with what we observed in the CRISPRi knockdown strains, where the spirochetes steadily maintained median lengths of 30-40 μm (**Fig. 3B-C**, **3F**, **3H**, and **3I**); the parental e2 strain had median lengths that spanned from 24-32 μm. The ranges

(maximum-minimum) of the cell lengths within these knockdown strains (147 µm, *dnaA*$_{T1}$; 134 µm, *dnaA*$_{NT1}$) were greater than that of the overexpression (77 µm) and parental (101 µm) bacteria.

When DnaA was overexpressed, the median cell length decreased by 2 days post-induction (**Fig. 3D**, **3H**, and **3K**). As cultures accumulated mutations in the overexpressed *dnaA*, cell lengths gradually increased to a peak at day 5, then decreased. This oscillation in spirochete length aligned with the observed growth pattern of this strain, where slowed replication corresponded to cells of shorter size and rapid replication to longer. This suggests that high levels of DnaA can diminish borrelial cell length. These results demonstrate that DnaA plays a role in regulating *B. burgdorferi* cell elongation and/or division and that maintaining proper DnaA levels is critical to these processes.

Impact of DnaA on ploidy and partitioning. *B. burgdorferi* is polyploid during exponential growth *in vitro* (27). As DnaA is the master initiator of chromosomal replication and affects *B. burgdorferi* morphology, we hypothesized that the ploidy and partitioning of chromosomes could be altered when DnaA levels are dysregulated. To test this, we transformed the parental e2 and *dnaA*$_{T1}$ strains with a construct expressing the chromosomal ParB protein fused to mCherry (pBSV2G_P$_{0826}$-mCherry$_{Bb}$-ParB), which has been demonstrated to bind near *oriC* (27). We first grew the two strains to mid-exponential phase without IPTG and measured the length and ParB-*oriC* puncta per cell. The parental bacteria were smaller than those of the uninduced *dnaA*$_{T1}$, consistent with our prior observations. Yet, both strains had similar numbers of ParB-*oriC* (**Fig. 4**). After taking these measurements, the *dnaA*$_{T1}$ culture was split in half, and IPTG was added to one of the cultures. The parental, uninduced, and induced strains were then incubated and examined for three more days.

On the first day post-induction, as the cultures entered stationary phase ($\geq 1x10^8$ cells/mL), all strains experienced a dramatic decline in the total ParB-*oriC* puncta per cell, consistent with prior observations (27). Over the next two days, the number of these continued to decrease in the parental and uninduced cultures, whereas the induced culture plateaued and ended with significantly more ParB-*oriC* puncta. Furthermore, the induced cell lengths, while longer than the parental, were the same as the uninduced cells, indicating the difference in puncta wasn't simply due to differences in cell length. With this, we concluded that depleting DnaA impairs the completion of borrelial chromosomal replication and cell division.

In addition to differences in the number of ParB-*oriC* puncta in the *dnaA*-conditional mutant, we also noted an apparent difference in their spacing (**Fig. 5A-B**) relative to the parental strain (**Fig. 5C**). Some cells had wide gaps between the foci, while others had foci that were close together. We assessed the cultures two- and three-days post-induction and found about 23.7% of parental e2 cells had irregular puncta spacing. The *dnaA*$_{T1}$ CRISPRi strains, in contrast, had significantly greater proportions of 53.8% and 55.3% of spirochetes with irregular spacing without and with added IPTG, respectively (**Fig. 5D**). Thus, knocking down DnaA also perturbs chromosomal partitioning.

Dysregulation of DnaA disrupts flagellar homeostasis. Depletion of DnaA also resulted in *B. burgdorferi* cells with aberrant helicity. Specifically, we observed spirochetes with a complete or partial loss of their characteristic corkscrew shape (**Fig. 6A** and **B**, respectively). Some of these tube-shaped cells were substantially elongated and showed evidence of incomplete division (**Fig. 6C** and **Supplemental Video**). About 13% of the spirochetes in the *dnaA*$_{T1}$-induced cultures and 8.7% of the uninduced exhibited abnormal morphologies (**Fig. 6D**). The parental and empty vector strains, independent of IPTG, did not exhibit such elevated

proportions of these cells, indicating that the observed helical abnormalities were due to targeted silencing of the *dnaA* gene. The high level of abnormal cells in the uninduced *dnaA*$_{T1}$ cultures, relative to the controls, can again be explained by leaky expression of the *dnaA* sgRNA encoded in the CRISPRi construct.

The characteristic corkscrew appearance of *B. burgdorferi* is due to the 7-11 flagella found in the periplasm (28). The motors that direct the movement of the endoflagella are normally localized to the bacterium's poles (29). The observed impacts on growth and partitioning suggest coordination between replication and flagellar assembly at the sites of division. This is not unheard of. In *E. coli*, for example, DnaA is known to be involved in flagellar regulation (30, 31).

DnaA is a global regulator of borrelial gene expression. DnaA is well known to be a transcription factor in many other bacteria, with regulons driving specific phenotypes (9). In *B. burgdorferi*, we previously demonstrated that DnaA controls the expression of the *dnaX-ebfC* operon (10). Considering this and the dramatic impacts of DnaA dysregulation on the Lyme spirochete, we queried whether the myriad phenotypes of the conditional mutants are due to DnaA-dependent transcriptional effects. To address this question, we performed RNA-seq on three strains with different levels of DnaA enrichment: wild-type (e2), DnaA-up (e2 + pACK121), and DnaA-down (e2 + *dnaA*$_{T1}$). All the strains had the plasmids cp26, lp17, lp54, cp32-1, cp32-3, and cp32-4, as assessed by PCR and whole genome sequencing. The bacteria for RNA-seq analysis were grown to mid-exponential phase, induced with 0.5 mM IPTG, and incubated overnight. We chose this strategy to mitigate the chance of escape-mutant development from confounding the results.

For the analyses of the RNA-seq data, comparisons were made between the three groups. We considered a gene to be differentially expressed if the false discovery rate (FDR) was less than or equal to 0.05 and had a $\log_2$FC (fold change) of ≥ 1 or ≤ -1. With these thresholds, 216 genes were noted as being differentially expressed between the wild-type and DnaA-down cultures (72 down, 144 up; **Fig. 7A**), 84 genes between WT and DnaA-up (40 down, 44 up; **Fig. 7B**), and 259 between DnaA-down and DnaA-up (105 down, 154 up; **Fig. 7C**). Principle component analysis showed that the replicates of each strain clustered together (**Fig. 7D**). Most of the genes that were differentially expressed are encoded on the chromosome: DnaA-down vs. e2: 69.9%; DnaA-up vs. e2: 72.6% (**Fig. 7E**). Of the plasmids, the linear lp54 replicon had the most impacted genes for the DnaA-down vs. e2 comparison (8.3%), while the circular cp32-1 had the most for the DnaA-up vs e2 comparison (7.1%; **Fig. 7E**).

As expected, the RNA-seq showed that compared to the e2 parent, *dnaA* transcript was about 2.8-fold less abundant in the CRISPRi strain and 15-fold more abundant in the overexpression strain. Typically, we normalize transcript levels to *ftsK*, a gene previously observed to have stable expression across growth phases (32). RNA-seq showed that *ftsK* was impacted by *dnaA* dysregulation (discussed below). Given this, we performed validations normalizing to *rpoB*, which did not change under the tested conditions. Using this approach, *dnaA* transcript was 80-fold less abundant in the knockdown vs. the WT and 16-fold more abundant in the overexpression vs. the WT (**Fig. 7E**). DnaA protein levels were about half as abundant in the knockdown and 13 times more in overexpression than the WT (**Fig. 10B**).

Transcript levels of many genes were most affected when *dnaA* levels were reduced. We initially hypothesized that transcriptomic profiles between the conditional mutants relative to the parental strain would reciprocally mirror each other. Only one gene fit this hypothesis, BB_0413

(2.2-fold increase for *dnaA*$_{T1}$/e2; 2.3-fold decrease for pACK121/e2). Indeed, in many cases, transcript levels for a gene would experience the same degree of change regardless of whether DnaA was increased or decreased. Such instances suggested that some of the observed changes in gene expression were not due to DnaA itself but rather a shared cellular response to the changes in DnaA levels. Despite some of these complications, the RNA-seq data set offered insights that could explain the phenotypes observed in the conditional *dnaA*-mutant strains.

The earliest interrogations into borrelial DnaA focused on its function as a transcription factor (10, 14). Consistent with our prior *in vitro* studies, knocking down *dnaA* significantly decreased transcription of the *dnaX-ebfC* operon (10). This operon codes for the τ-subunit of the DNA polymerase III holoenzyme (DnaX) and the nucleoid-associated protein, EbfC. Other impacted replication genes included the DNA polymerase III β-clamp (*dnaN*), DNA polymerase I (*polA*), DNA topoisomerase IV (*parEC*), and telomere resolvase (*resT*). Except for *dnaN*, these genes were downregulated when *dnaA* levels were decreased. The upregulation of *dnaN*, seen when comparing DnaA-Up to DnaA-down conditions, suggests that DnaA represses the expression of this gene. This possibility is unsurprising given that the *oriC* is directly 5' of the *dnaN* ORF, and we have shown that DnaA binds this region (10).

In the *dnaA*-knockdown *B. burgdorferi*, we observed cells that were considerably elongated. In our evaluation of the borrelial genome, we identified 22 homologs of genes that encode components of either the bacterial elongasome or divisome (**Table 1**). Of these, 39.1% were differentially expressed in the *dnaA*$_{T1}$ CRISPRi strain (**Fig. 8A**). Among these were *mreB*, *mreC*, *mreD,* and *mrdA*, which constitute an apparent operon and encode core components of the bacterial elongasome (**Fig. 8B**). MreB is an actin-like cytoskeleton protein that polymerizes across the bacterial inner membrane to regulate the spatiotemporal peptidoglycan synthesis of

growing cells (33-35). Knockdown of MreB in *B. burgdorferi* results in bulging and cell widening at the division sites (19). MreC and MreD are membrane-embedded proteins that interact and regulate the peptidoglycan crosslinking activity of PBP2 (penicillin-binding protein 2; MrdA) (36). The peptidoglycan polymerase RodA and PBP1a interact with PBP2, with the former stimulating its activity. Except for *mreD*, the genes in the apparent *mre* operon were downregulated in *dnaA*-deficient *B. burgdorferi*. A DNA sequence that is the same as those found in the *oriC*, which may constitute the borrelial DnaA-box, is located upstream of the *mreB* ORF, suggesting DnaA may directly regulate the expression of these genes. The decreased transcript levels for *mreB*, *mreC*, and *mrdA* would suggest decreased elongation, which is the opposite of what we observed (**Fig. 3**). This apparent contradiction suggests that filamentation may be due to defects in cell division.

The transcripts of four important divisome proteins were impacted when *dnaA* was knocked down: FtsA, FtsK, FtsE, and FtsX (**Fig. 8A** and **B**). FtsA is the membrane anchor protein for the septation marker protein FtsZ (37, 38), and its transcript increased about 2-fold in the conditional *dnaA* mutant. Surprisingly, DnaA-overexpressed *B. burgdorferi* also experienced a 2-fold increase in *ftsA*. Transcripts for FtsK, the DNA translocase, declined 2-fold. FtsE and FtsX, encoded next to each other, had their transcripts decreased 2-fold and increased almost 3-fold, respectively. Interestingly, a second allele of *ftsX* (*ftsX**), which is truncated, is located directly upstream of *ftsEX,* and transcript levels of this gene were substantially affected, with a 189-fold increase. Like the *mre* locus, DnaA could regulate these genes directly as potential DnaA-boxes are adjacent to these loci.

In the conditional *dnaA*-knockdown *B. burgdorferi,* we observed spirochetes that had lost their helical structure and hypothesized these cells had disrupted flagella. The *B. burgdorferi*

genome encodes nearly three dozen flagellar genes (**Fig. 9A**). When *dnaA* was knocked down, six of these genes were significantly impacted: *fliQ*, *fliR*, *flgD*, *flaA*, *flgV*, and *flgA* (**Fig. 9B**). All these genes except for *flaA* and *flgA* are encoded in the *flgB* superoperon. FliQ and FliR are components of the flagellar export apparatus (39). FlgD is a scaffolding protein that is required for flagellar hook formation (40, 41). FlaA is the minor borrelial flagellar filament protein (42, 43). FlgV is a protein first characterized as a homolog of the RNA chaperone Hfq, but recent work has demonstrated the protein localizes with flagellar motors and modulates their assembly (44, 45). FlgA is a chaperone involved in the formation of the P-ring of the flagellar motor (46). The transcripts for *fliR* and *flgD* increased the most of these genes, about 15 and 4-fold, respectively, when DnaA levels were reduced. The changes in the expression of these genes could alter flagellar assembly homeostasis and explain the observed abnormalities in helicity in the *dnaA*-deficient spirochetes. It is also possible that defects in septation disrupted the localization and assembly of flagella.

In addition to affecting genes for essential cellular processes, DnaA significantly impacted the expression of outer surface proteins that are involved in vertebrate infection and virulence, such as ErpA, decorin binding protein DbpA, and OspC (**Fig. 7A-C** and **Fig. 10E-F**). The Erps are multifunctional adhesins that bind vertebrate host factors such as laminin, plasminogen, and complement proteins (47-52). Transcripts for *erpA* increased in the *dnaA* knockdown and overexpression conditions (**Fig. 10E-F**). Interestingly, this increase in transcript didn't correspond to increased ErpA protein (**Fig. 10B-D**).

The *erp* genes are encoded on the cp32 plasmids and have conserved operators that allow uniform regulation (53). The Erps are turned on when the tick begins to feed, a time of rapid borrelial replication, and remain on during vertebrate infection (54). Three proteins bind the *erp*

operators and regulate their expression: BpaB (Borrelial cp32 ParB analog), BpuR, and EbfC. BpaB represses *erp* transcription along with the co-repressor BpuR (**Fig. 10A**) (55-57). EbfC is the antirepressor that antagonizes BpaB to allow for *erp* transcription (56). DnaA was previously hypothesized to regulate *erp* transcription by activating EbfC and repressing BpuR (10, 13, 14). EbfC transcript and protein levels decreased when *dnaA* was knocked down, consistent with that model (**Fig. 10B** and **E**). BpuR transcript, however, did not significantly change, but its protein levels appeared to decline with a decrease in cellular DnaA concentrations (**Fig. 10B** and **E**). BpuR alone does not repress *erp* expression, so this cannot account for the increase in ErpA transcript. Thus, we looked at the protein levels of the *erp* repressor. Despite the lack of a change in the transcript, immunoblots showed a decrease in BpaB protein levels in *dnaA* CRISPRi *B. burgdorferi*, which can explain the increase in *erpA* transcript (**Fig. 10B, C,** and **E**). BpaB levels were similar to those of the parental e2 strain during *dnaA* overexpression, and ErpA transcript and protein were unaffected, likely due to normal levels of the antirepressor EbfC. Overall, these results demonstrate that DnaA not only affects the expression of genes involved in basic cellular processes but also those involved in maintaining the Lyme spirochete's infection cycle.

DISCUSSION

In this study, we sought to understand the roles of DnaA in controlling the physiology of *B. burgdorferi*. To do this, we utilized inducible CRISPRi and overexpression vectors. Overexpressing DnaA was toxic to the bacteria and was consistently overcome by mutations in the inducible *dnaA*. This, along with the difference in DnaA levels from overexpression vs. knockdown, 13-fold DnaA increase vs. 2-fold decrease, likely explains some of the results we encountered. Nevertheless, increasing DnaA levels yielded significantly different phenotypes, such as spirochete size. CRISPRi was the more reliable and effective means of producing conditional *dnaA* mutants in *B. burgdorferi*. This approach targeting *dnaA* has been successfully described in *E. coli*, *Lactobacillus plantarum,* and *Streptococcus pyogenes* (58-60). An attempt was made in *Pseudomonas putida,* but clones couldn't be recovered (61).

We found that lowering the cellular levels of DnaA profoundly reduced cell division, consistent with the protein's function as the chromosomal replication initiator. The reduction of DnaA also coincided with decreased expression of many essential replication genes. It is known that one of these genes, *dnaX*, is directly regulated by DnaA (10). This suggests that DnaA may directly regulate those other genes, or *B. burgdorferi* may have mechanisms to sense replication initiation and coordinate gene expression accordingly.

DnaA-deficient spirochetes also increased in length. The bacterial cell cycle is typically divided into three phases: B, C, and D (62). The B and D phases correspond to the birth and division of the bacteria, respectively. The C phase corresponds to everything in between, namely, chromosomal replication, along with elongation/growth. Replication is initiated by DnaA and then carried out by the replisome. Elongation is facilitated by the elongasome, which synthesizes peptidoglycan to allow for cell growth. The DnaA-depleted spirochetes, although considerably

longer than the parental strain, had overall decreased expression of elongasome genes, the *mre* locus in particular. This suggested a division issue, but we cannot rule out the possibility that DnaA is required for cross-talk between replication and cell growth. Indeed, it is likely that replication, elongation, and division are all interconnected. Lyme and relapsing *Borreliae* elongate at three distinct zones along their length: 1/4, 1/2, and 3/4 (63). This localization pattern at the mid-cell suggests an interplay between elongation and division machinery. How or if DnaA directly plays into this delicate balance remains to be assessed.

Many bacterial cell division proteins are denoted "Fts" for their filamentous phenotypes caused by temperature-sensitive mutations (64). Knocking down DnaA affected the expression of *ftsA*, *ftsEX*, and *ftsK*. The dysregulation of these genes potentially explains both the elongated phenotype and the irregular spacing of the ParB-*oriC* puncta.

FtsA localizes to the inner leaflet of the inner membrane and binds FtsZ. Increased FtsA, seen when DnaA was knocked down, could decrease Z-ring assembly and, thus, cytokinesis. In *E. coli*, overexpression of FtsA causes cells to filament (65). Overexpressed DnaA spirochetes had elevated *ftsA* transcript, but no changes were observed in *ftsEX*. The FtsEX complex regulates the activity of peptidoglycan hydrolases and FtsA (66-69). Disruption of FtsE and FtsX levels could, therefore, prevent the breakdown of peptidoglycan and Z-ring formation at the site of division. The combined perturbation of *ftsA* and *ftsEX* expression in the *dnaA* CRISPRi strain potentially explains the observed elongated phenotype.

In addition to changes in spirochete length in the DnaA-depleted *B. burgdorferi*, we observed abnormal spacing of ParB-*oriC* puncta. These bacteria had decreased transcripts of the membrane-embedded DNA translocase FtsK, a core component of the divisome (70-72). FtsK, through its C-terminal αβγ-domain, resolves chromosome dimers and translocates DNA from the

septum to allow for cytokinesis (73-76). A decrease in FtsK could thus result in the failure to separate sister chromosomes, leading to cells with abnormal ploidy. This could also explain why some *oriC* sites were located close together in the *dnaA* knockdown strain (**Fig. 5**). FtsK also recruits downstream divisome proteins through its N-terminal transmembrane domain (71, 77-79). Therefore, reducing FtsK may also limit the recruitment of divisome proteins to the septa.

Motility is perhaps the most important "virulence" factor that *B. burgdorferi* employs to infect and colonize its vertebrate hosts. By knocking down DnaA in the Lyme spirochete, we observed a substantial impact on the bacteria's helicity. This corkscrew morphology is due to periplasmic flagella (28). Key genes, such as FlgD and FliR, were overexpressed when levels of DnaA were lowered. FliR is a component of the flagellar motor's export apparatus, which transports flagellar filament substrates from the cytoplasm to the periplasm (39). Disrupting the balance of this subunit would very likely impair the overall function and structure of the flagellar motor and filament. By increasing FliR, it is possible that the export of the flagellar cargo to the periplasmic space would be affected, which in turn would prevent flagella formation. The flagellar motors are normally localized to the poles and developing septa of *B. burgdorferi*. This suggests that replication, elongation, or division processes may coordinate the formation of flagellar motors at the dividing mid-cell. In *E. coli*, DnaA regulates genes involved in flagellar assembly (30, 31, 80). Whether DnaA in *B. burgdorferi* acts through a similar mechanism is unknown.

In addition to the many morphological changes incurred by dysregulation of DnaA, there were also significant impacts on the expression of vertebrate infection-related outer surface proteins. Many of these antigenic proteins, such as OspC, DbpA, and the Erps are turned on during the tick blood meal, a period defined by rapid replication. Relative to these genes, levels

of transcript for the alternative sigma factor RpoS were not significantly changed by manipulation of DnaA levels. We previously demonstrated that DnaA regulates the *erp* antirepressor EbfC and may regulate the *erp* co-repressor BpuR (10, 14). With our CRISPRi approach, we were able to validate our prior data on *dnaX-ebfC* regulation. While we could not detect any substantial differences in BpuR with DnaA manipulation, this might have been a consequence of assessing mid-exponential spirochetes grown at 34 ºC; BpuR expression is highest when grown at 23 ºC (14, 57). When DnaA levels were reduced, expression of ErpA increased. We suggest this could be due to decreased levels of *erp* repressor BpaB. While this was unexpected, it is logical that a partitioning protein be decreased when *dnaA* transcription is knocked down. This suggests that these extrachromosomal DNAs can sense changes in chromosomal replication. How this is mediated remains to be investigated.

We observed gene expression level changes in a vast number of regulatory networks. This led us to examine if *dnaA* knockdown or overexpression impacted any known regulatory factors. Among the known networks, we observed modest changes in gene expression levels of the following regulators: Hk1, Rrp1, and SpoVG. These changes did not meet the log fold change threshold but were significant (FDR ≤ 0.05) and had a log fold change of approximately 1.5. When comparing the *dnaA*$_{T1}$ knockdown strain to the parental e2 strain, these genes were downregulated by a fold change of 1.52, 1.61, and 1.53, respectively. While not meeting our set threshold, it is possible the combined modest expression changes in these regulators considerably impacted the expression levels of the genes they modulate. For example, the nucleic acid binding protein SpoVG, the response regulator Hk1, and diguanylate cyclase Rrp1 are all known to regulate the glycerol metabolism (*glpFKD*) operon, which is essential for *B. burgdorferi* colonization and persistence in ticks (81-85). The downregulation of the *glpFKD* operon (~2.6 to

4-fold) is likely attributable to the decreased expression of *spoVG*, *hk1*, and *rrp1*. These observations link DnaA and/or DNA replication to crucial borrelial networks, including the c-di-GMP regulatory network (Hk1/Rrp1) critical to completing the *B. burgdorferi* enzootic life cycle.

Another regulatory network impacted was the Hk2/Rrp2 pathway, whose expression levels were increased by 8.2 and 1.5, respectively. The Hk2/Rrp2 two-component system is a known activator of the RpoN/RpoS alternative sigma factor cascade, which regulates essential virulence factors like OspC (86-88). Deletion of *rrp2* is lethal, and investigations into *rrp2* regulation have relied on conditional mutants (18). Although neither *rpoN* nor *rpoS* levels changed significantly, we note that *rpoS* transcription can be activated by the housekeeping sigma factor RpoD in addition to RpoN (89). This further provides strong evidence that the Hk2/Rrp2 pathway has impacts outside of *rpoS* regulation potentially mediated by proper *dnaA* levels and/or associated with DNA replication. In addition, this data supports our past data showing that *ospC* regulation, through the repressor Gac, can occur independently of RpoS regulation (90). Additional data from our lab indicates that DnaA is a positive activator of OspC (unpublished results). This supports the RNA-seq data in this study, showing that knockdown of DnaA levels reduces *ospC* transcript.

Organisms have evolved complex and varied molecular circuits to regulate cellular homeostasis in ever-changing environments. Bacterial pathogens, especially, have developed such networks in their tussle against host defenses. During the tick blood meal, *B. burgdorferi* must take advantage of the nutrients to propagate its numbers, reprogram its transcriptome, and disseminate to the vertebrate. Failure to do so means death, as *B. burgdorferi* cannot be transmitted vertically to tick offspring (91). In *B. burgdorferi,* DnaA, the master regulator of

437 replication initiation, appears to form a complex regulatory network to coordinate these essential
438 processes (**Fig. 11**). Future studies need to be conducted to determine which of the DnaA-
439 dysregulated effects described here are due to DnaA itself or a consequence of a lack of initiation
440 of chromosomal replication.

441

442 METHODS AND MATERIALS.

443 **Bacterial strains, plasmids, and genetic manipulations.** Studies were conducted using
444 the readily transformable *B. burgdorferi* clonal strain B31-e2 (92). Spirochetes were grown in
445 liquid Barbour-Stoener-Kelly II (BSK-II) medium supplemented with 6% rabbit serum (v/v) at
446 35 ºC. For all experiments, *B. burgdorferi* was diluted from mid-exponential phase (3-5 x 10^7
447 cells/mL) into fresh BSK-II medium. Cultures were only used if they were at least two passages
448 away and no more than three from the initial -80ºC stock. Borrelial culture densities were
449 enumerated using a Petroff-Hauser counting chamber and dark-field microscopy.

450 The *dnaA* overexpression (pACK121) and CRISPRi plasmids (pACK136, $dnaA_{T1}$;
451 pACK138, $dnaA_{NT1}$) were generated by GenScript. The pACK121 plasmid is a derivative of
452 pJSB268 (17). The plasmid was designed to replace the *luc* gene with the *B. burgdorferi dnaA*
453 gene containing an N-terminal 3xFLAG epitope. The pACK136 ($dnaA_{T1}$) and pACK137
454 ($dnaA_{NT1}$) plasmids are derivatives of pJJW101 (20). These plasmids were created by inserting
455 the desired sgRNA sequence between the BsaI sequences. The sgRNA targets used in this study
456 were chosen using CRISPy-web (https://crispy.secondarymetabolites.org) and B31 chromosome
457 contig (NC_001318). Whole-plasmid sequencing was performed by Plasmidsaurus using Oxford
458 Nanopore Technology with custom analysis and annotation.

Growth curve analysis. Growth curves for each strain were generated from three independent experiments. Cultures were seeded at the same initial density (1 or 5 x 10^5 cells/mL) and enumerated over seven days. Generation times were calculated in Microsoft Excel by fitting an exponential curve to the data points denoting the beginning and end of logarithmic growth. Statistically significant differences were determined by one-way ANOVA.

Immunoblot analyses. Polyclonal DnaA antibodies were generated by Thermo Scientific in rabbits using recombinant GST-DnaA generated in-house (10). The serum from the final bleed was purified by affinity purification using MBP-DnaA on an amylose column. Murine monoclonal anti-FlaB antibodies were used to assess the even loading of SDS-PAGE gels (93). Other primary antibodies were generated previously (56, 57, 94). Cells for immunoblot were pelleted and washed three times with 1x PBS, pH 7.4. Approximately 10^7 spirochetes were loaded per lane for SDS-PAGE. Goat anti-Rabbit Alexa Fluor 488 (1:10, 000, Thermo Scientific) and Goat anti-Mouse IRDye800 (1:5,000, Licor) were used as secondary antibodies. Densitometric analyses were performed using ImageLab software (BioRad). The intensities of the bands of interest were normalized to the corresponding loading control.

Quantitative reverse transcription-PCR (qRT-PCR). Mid-exponential phase (3-5 x 10^7 cells/mL) bacteria were washed three times with PBS (pH 7.4) before RNA extraction using Qiagen Mini RNA kits. Genomic DNA was cleared by on-column DNase treatment. RNA was reverse transcribed using iScript cDNA synthesis kits (Bio-Rad). Quantitative PCR was conducted using iTaq Universal SYBR Green Supermix (Bio-Rad) and a Bio-Rad CFX96 Touch Real-time PCR thermocycler. The primer sets used for this study were designed using the IDT Primer Quest Tool (https://www.idtdna.com/PrimerQuest/Home/Index). Cq values were normalized to *ftsK* or *rpoB* (ΔCq) and then to the parental strain or uninduced control (ΔΔCq).

Fold expression was determined using the function $2^{-\Delta\Delta Cq}$. If $\Delta\Delta Cq > 0$, then the function $-2^{\Delta\Delta Cq}$ was used.

Cell length analysis. Wet mounts of live bacteria were visualized by dark-field with an Olympus Bx51 microscope at 400x total magnification. Micrographs were taken using a C-mounted Accu-scope Excelis HD camera. Cell lengths were determined using Captavision+ software. A conversion factor of 13.80 pixels/µm was used for all measurements. For each replicate and time point, approximately 50 spirochetes were measured.

Fluorescence microscopy and image analysis. Spirochetes were pelleted by centrifugation, washed twice with PBS (pH 7.4), and diluted to a final concentration of 1 x 10^5 cells/mL. Ten microliters of cells were mounted on a glass slide. Cells were visualized using an Olympus Bx51 microscope with a Cool LED p-E300 illumination system. Micrographs of dark-field and red fluorescence were captured for each field of view using a C-mounted Accu-scope Excelis HD camera. Micrographs were merged in ImageJ, and the background was inverted using EZreverse (https://amsterdamstudygroup.shinyapps.io/ezreverse/) with the HSL color space option (95).

Whole Genome Sequencing (WGS) and analysis. The parental *B. burgdorferi* B31-e2, *dnaA*$_{T1}$ CRISPRi, and *dnaA*-overexpression strains were sequenced to verify plasmid content and determine if mutations occurred in the *dnaA* sequence of the generated strains. Briefly, the strains were grown in duplicate to mid-exponential phase (3-5 x 10^7 cells/mL). Two mLs of cells were pelleted and washed twice with PBS (pH 7.4) and frozen at -80 ºC. DNA extraction and whole genome sequencing were performed by SeqCenter. Briefly, the cells were sent to the SeqCenter facility. DNA was extracted from the pellets using the ZymoBIOMICS™ DNA

Miniprep Kit according to the manufacturer's protocol. DNA concentrations were determined by Qubit.

Sequencing libraries were prepared via the tagmentation-based and PCR-based Illumina DNA Prep kit and custom IDT 10 bp unique dual indices (UDI) with a target insert size of 320 bp. The sequencing was performed either in one or more multiplexed flow-cell runs on an Illumina NovaSeq 6000 sequencer resulting in 2x151 bp paired-end reads. Quality control steps including demultiplexing and adapter trimming were performed with bcl-convert (v4.1.5). Reads were aligned to the *B. burgdorferi* B31 genome assembly (GCF_000008685.2_ASM868v2). Variant calling was performed using BreSeq (v. 0.38.1) under default settings.

RNA sequencing (RNA-seq) and analysis. The same cultures of the parental *B. burgdorferi* B31-e2, *dnaA*$_{T1}$ CRISPRi, and *dnaA*-overexpression strains used for WGS were used for RNA-seq. All strains were grown in duplicate to mid-exponential growth phase (3-5 x 10^7 cells/mL) and induced with 0.5 mM IPTG overnight at 35 ºC. Nine mLs of the cells were pelleted and washed two times with PBS (pH 7.4) and frozen at -80 ºC. The cells were sent to SeqCenter for RNA extraction and sequencing using their intermediate RNA analysis with replicates (Prokaryotic) service. Briefly, their method consisted of quality control and adapter trimming by bclconvert (version 4.1.5) and mapping reads using HISAT2 (version 2.2.0) to the RefSeq version of the *B. burgdorferi* B31 genome assembly (GCF_000008685.2_ASM868v2). The read counts were uploaded into R (version 4.0.2) and normalized using the edgeR Trimmed Mean of M values (TMM) algorithm (1.14.5). Differential gene expression analysis was performed with edgeR using the normalized TMM values. Only plasmids that were confirmed to be present were included in the analyses. We further filtered the data set by setting the thresholds for differential expression at $\log_2$FC ≥ 1 or ≤ -1 and an FDR ≤ 0.05. Differentially expressed

527 genes (DEGs) were visualized via volcano plots made using VolcaNoseR (96). DEGs belonging
528 to the elongasome and divisome were visualized by heatmap. The heatmap was generated in R (v
529 4.4.1) using the pheatmap package, with the log2 transformed normalized counts per million
530 (CPMs) (97). The clustering method used for the heatmap was the default method of complete
531 linkage, while the distance measure used was correlation.

532 To identify flagellar, cell division, and elongation homologs, the genome was directly
533 searched for annotations, or the sequences of characterized proteins from other bacteria were
534 aligned by BLAST against the *B. burgdorferi* genome.

535

Acknowledgments

This research was funded by NIH grant R21 AI147139. We thank Dr. Wolfram Zückert and Bryan Murphy for their help designing and troubleshooting the CRISPRi shuttle vectors and Dr. Jon Blevins for providing the pJSB268 shuttle vector. BioRender was used to make the schematics in Figures 1, 2, 8, 9, and 10.

Works Cited.

1. Radolf JD, Caimano MJ, Stevenson B, Hu LT. 2012. Of ticks, mice and men: understanding the dual-host lifestyle of Lyme disease spirochaetes. Nat Rev Microbiol 10:87-99.
2. Steere AC, Strle F, Wormser GP, Hu LT, Branda JA, Hovius JW, Li X, Mead PS. 2016. Lyme borreliosis. Nat Rev Dis Primers 2:16090.
3. De Silva AM, Fikrig E. 1995. Growth and migration of *Borrelia burgdorferi* in *Ixodes* ticks during blood feeding. Am J Trop Med Hyg 53:397-404.
4. Piesman J, Oliver JR, Sinsky RJ. 1990. Growth kinetics of the Lyme disease spirochete (*Borrelia burgdorferi*) in vector ticks (*Ixodes dammini*). Am J Trop Med Hyg 42:352-7.
5. Speck C, Messer W. 2001. Mechanism of origin unwinding: sequential binding of DnaA to double- and single-stranded DNA. EMBO J 20:1469-76.
6. Kaur G, Vora MP, Czerwonka CA, Rozgaja TA, Grimwade JE, Leonard AC. 2014. Building the bacterial orisome: high-affinity DnaA recognition plays a role in setting the conformation of *oriC* DNA. Mol Microbiol 91:1148-63.
7. Ozaki S, Katayama T. 2012. Highly organized DnaA-*oriC* complexes recruit the single-stranded DNA for replication initiation. Nucleic Acids Res 40:1648-65.
8. Messer W, Weigel C. 1997. DnaA initiator--also a transcription factor. Mol Microbiol 24:1-6.
9. Menikpurage IP, Woo K, Mera PE. 2021. Transcriptional Activity of the Bacterial Replication Initiator DnaA. Front Microbiol 12:662317.

562 10. Krusenstjerna AC, Saylor TC, Arnold WK, Tucker JS, Stevenson B. 2023. *Borrelia*
563 *burgdorferi* DnaA and the Nucleoid-Associated Protein EbfC Coordinate Expression of
564 the *dnaX-ebfC* Operon. J Bacteriol 205:e0039622.
565 11. Medrano MS, Ding Y, Wang X-G, Lu P, Coburn J, Hu LT. 2007. Regulators of
566 expression of the oligopeptide permease A proteins of *Borrelia burgdorferi*. Journal of
567 bacteriology 189:2653-2659.
568 12. Jutras BL, Bowman A, Brissette CA, Adams CA, Verma A, Chenail AM, Stevenson B.
569 2012. EbfC (YbaB) is a new type of bacterial nucleoid-associated protein and a global
570 regulator of gene expression in the Lyme disease spirochete. J Bacteriol 194:3395-406.
571 13. Stevenson B, Krusenstjerna AC, Castro-Padovani TN, Savage CR, Jutras BL, Saylor TC.
572 2022. The Consistent Tick-Vertebrate Infectious Cycle of the Lyme Disease Spirochete
573 Enables Borrelia burgdorferi To Control Protein Expression by Monitoring Its
574 Physiological Status. J Bacteriol 204:e0060621.
575 14. Jutras BL, Savage CR, Arnold WK, Lethbridge KG, Carroll DW, Tilly K, Bestor A, Zhu
576 H, Seshu J, Zuckert WR, Stewart PE, Rosa PA, Brissette CA, Stevenson B. 2019. The
577 Lyme disease spirochete's BpuR DNA/RNA-binding protein is differentially expressed
578 during the mammal-tick infectious cycle, which affects translation of the SodA
579 superoxide dismutase. Mol Microbiol 112:973-991.
580 15. Picardeau M, Lobry JR, Hinnebusch BJ. 1999. Physical mapping of an origin of
581 bidirectional replication at the centre of the *Borrelia burgdorferi* linear chromosome. Mol
582 Microbiol 32:437-45.

16. Hirota Y, Ryter A, Jacob F. 1968. Thermosensitive mutants of *E. coli* affected in the processes of DNA synthesis and cellular division. Cold Spring Harb Symp Quant Biol 33:677-93.

17. Blevins JS, Revel AT, Smith AH, Bachlani GN, Norgard MV. 2007. Adaptation of a luciferase gene reporter and *lac* expression system to *Borrelia burgdorferi*. Appl Environ Microbiol 73:1501-13.

18. Groshong AM, Gibbons NE, Yang XF, Blevins JS. 2012. Rrp2, a prokaryotic enhancer-like binding protein, is essential for viability of *Borrelia burgdorferi*. J Bacteriol 194:3336-42.

19. Takacs CN, Scott M, Chang Y, Kloos ZA, Irnov I, Rosa PA, Liu J, Jacobs-Wagner C. 2020. A CRISPR interference platform for selective downregulation of gene expression in *Borrelia burgdorferi*. Appl Environ Microbiol doi:10.1128/AEM.02519-20.

20. Murphy BT, Wiepen JJ, He H, Pramanik AS, Peters JM, Stevenson B, Zuckert WR. 2023. Inducible CRISPRi-Based Operon Silencing and Selective in Trans Gene Complementation in *Borrelia burgdorferi*. J Bacteriol 205:e0046822.

21. Zheng W, Li Z, Skarstad K, Crooke E. 2001. Mutations in DnaA protein suppress the growth arrest of acidic phospholipid-deficient *Escherichia coli* cells. EMBO J 20:1164-72.

22. Jonas K, Chen YE, Laub MT. 2011. Modularity of the bacterial cell cycle enables independent spatial and temporal control of DNA replication. Curr Biol 21:1092-101.

23. Anderson ME, Smith JL, Grossman AD. 2022. Multiple mechanisms for overcoming lethal over-initiation of DNA replication. Mol Microbiol 118:426-442.

605 24. Cooper S, Helmstetter CE. 1968. Chromosome replication and the division cycle of
606 *Escherichia coli* Br. Journal of Molecular Biology 31:519-540.
607 25. Donachie WD. 1968. Relationship between Cell Size and Time of Initiation of DNA
608 Replication. Nature 219:1077-1079.
609 26. Wallden M, Fange D, Lundius EG, Baltekin Ö, Elf J. 2016. The Synchronization of
610 Replication and Division Cycles in Individual *E. coli* Cells. Cell 166:729-739.
611 27. Takacs CN, Wachter J, Xiang Y, Ren Z, Karaboja X, Scott M, Stoner MR, Irnov I,
612 Jannetty N, Rosa PA, Wang X, Jacobs-Wagner C. 2022. Polyploidy, regular patterning of
613 genome copies, and unusual control of DNA partitioning in the Lyme disease spirochete.
614 Nat Commun 13:7173.
615 28. Motaleb MA, Corum L, Bono JL, Elias AF, Rosa P, Samuels DS, Charon NW. 2000.
616 *Borrelia burgdorferi* periplasmic flagella have both skeletal and motility functions. Proc
617 Natl Acad Sci U S A 97:10899-904.
618 29. Li C, Bakker RG, Motaleb MA, Sartakova ML, Cabello FC, Charon NW. 2002.
619 Asymmetrical flagellar rotation in *Borrelia burgdorferi* nonchemotactic mutants. Proc
620 Natl Acad Sci U S A 99:6169-74.
621 30. Wu D, Baigalmaa L, Yao Y, Li G, Su M, Fan L, Morigen. 2021. The *Escherichia coli*
622 QseB/QseC signaling is required for correct timing of replication initiation and cell
623 motility. Gene 773:145374.
624 31. Mizushima T, Tomura A, Shinpuku T, Miki T, Sekimizu K. 1994. Loss of flagellation in
625 *dnaA* mutants of *Escherichia coli*. J Bacteriol 176:5544-6.
626 32. Arnold WK, Savage CR, Brissette CA, Seshu J, Livny J, Stevenson B. 2016. RNA-Seq of
627 *Borrelia burgdorferi* in Multiple Phases of Growth Reveals Insights into the Dynamics of

628 Gene Expression, Transcriptome Architecture, and Noncoding RNAs. PLoS One
629 11:e0164165.
630 33. Jones LJ, Carballido-Lopez R, Errington J. 2001. Control of cell shape in bacteria:
631 helical, actin-like filaments in *Bacillus subtilis*. Cell 104:913-22.
632 34. Kruse T, Bork-Jensen J, Gerdes K. 2005. The morphogenetic MreBCD proteins of
633 *Escherichia coli* form an essential membrane-bound complex. Mol Microbiol 55:78-89.
634 35. Figge RM, Divakaruni AV, Gober JW. 2004. MreB, the cell shape-determining bacterial
635 actin homologue, co-ordinates cell wall morphogenesis in *Caulobacter crescentus*. Mol
636 Microbiol 51:1321-32.
637 36. Liu X, Biboy J, Consoli E, Vollmer W, den Blaauwen T. 2021. MreC and MreD balance
638 the interaction between the elongasome proteins PBP2 and RodA. PLOS Genetics
639 16:e1009276.
640 37. Pichoff S, Lutkenhaus J. 2005. Tethering the Z ring to the membrane through a conserved
641 membrane targeting sequence in FtsA. Mol Microbiol 55:1722-34.
642 38. Pichoff S, Lutkenhaus J. 2002. Unique and overlapping roles for ZipA and FtsA in septal
643 ring assembly in *Escherichia coli*. Embo j 21:685-93.
644 39. Minamino T, Macnab RM. 1999. Components of the *Salmonella* flagellar export
645 apparatus and classification of export substrates. J Bacteriol 181:1388-94.
646 40. Kutsukake K, Doi H. 1994. Nucleotide sequence of the *flgD* gene of *Salmonella*
647 *typhimurium* which is essential for flagellar hook formation. Biochim Biophys Acta
648 1218:443-6.
649 41. Ohnishi K, Ohto Y, Aizawa S, Macnab RM, Iino T. 1994. FlgD is a scaffolding protein
650 needed for flagellar hook assembly in *Salmonella typhimurium*. J Bacteriol 176:2272-81.

651 42. Ge Y, Li C, Corum L, Slaughter CA, Charon NW. 1998. Structure and expression of the
652 FlaA periplasmic flagellar protein of *Borrelia burgdorferi*. J Bacteriol 180:2418-25.
653 43. Motaleb MA, Sal MS, Charon NW. 2004. The decrease in FlaA observed in a *flaB*
654 mutant of Borrelia burgdorferi occurs posttranscriptionally. J Bacteriol 186:3703-11.
655 44. Lybecker MC, Abel CA, Feig AL, Samuels DS. 2010. Identification and function of the
656 RNA chaperone Hfq in the Lyme disease spirochete *Borrelia burgdorferi*. Mol Microbiol
657 78:622-35.
658 45. Zamba-Campero M, Soliman D, Yu H, Lasseter AG, Chang Y-Y, Liu J, Aravind L,
659 Jewett MW, Storz G, Adams PP. 2024. Broadly conserved FlgV controls flagellar
660 assembly and *Borrelia burgdorferi* dissemination in mice. bioRxiv
661 doi:10.1101/2024.01.09.574855:2024.01.09.574855.
662 46. Juhas M, Ajioka JW. 2015. Identification and validation of novel chromosomal
663 integration and expression loci in *Escherichia coli* flagellar region 1. PLoS One
664 10:e0123007.
665 47. Stevenson B, Brissette CA. 2023. Erp and Rev Adhesins of the Lyme Disease
666 Spirochete's Ubiquitous cp32 Prophages Assist the Bacterium during Vertebrate
667 Infection. Infect Immun 91:e0025022.
668 48. Stevenson B, El-Hage N, Hines MA, Miller JC, Babb K. 2002. Differential binding of
669 host complement inhibitor factor H by *Borrelia burgdorferi* Erp surface proteins: a
670 possible mechanism underlying the expansive host range of Lyme disease spirochetes.
671 Infect Immun 70:491-7.

672 49. Brissette CA, Haupt K, Barthel D, Cooley AE, Bowman A, Skerka C, Wallich R, Zipfel
673 PF, Kraiczy P, Stevenson B. 2009. *Borrelia burgdorferi* infection-associated surface
674 proteins ErpP, ErpA, and ErpC bind human plasminogen. Infect Immun 77:300-6.
675 50. Brissette CA, Verma A, Bowman A, Cooley AE, Stevenson B. 2009. The *Borrelia*
676 *burgdorferi* outer-surface protein ErpX binds mammalian laminin. Microbiology
677 (Reading) 155:863-872.
678 51. Garrigues RJ, Thomas S, Leong JM, Garcia BL. 2022. Outer surface lipoproteins from
679 the Lyme disease spirochete exploit the molecular switch mechanism of the complement
680 protease C1s. J Biol Chem 298:102557.
681 52. Pereira MJ, Wager B, Garrigues RJ, Gerlach E, Quinn JD, Dowdell AS, Osburne MS,
682 Zückert WR, Kraiczy P, Garcia BL, Leong JM. 2022. Lipoproteome screening of the
683 Lyme disease agent identifies inhibitors of antibody-mediated complement killing. Proc
684 Natl Acad Sci U S A 119:e2117770119.
685 53. Babb K, McAlister JD, Miller JC, Stevenson B. 2004. Molecular characterization of
686 *Borrelia burgdorferi erp* promoter/operator elements. J Bacteriol 186:2745-56.
687 54. Miller JC, von Lackum K, Babb K, McAlister JD, Stevenson B. 2003. Temporal analysis
688 of *Borrelia burgdorferi* Erp protein expression throughout the mammal-tick infectious
689 cycle. Infect Immun 71:6943-52.
690 55. Burns LH, Adams CA, Riley SP, Jutras BL, Bowman A, Chenail AM, Cooley AE,
691 Haselhorst LA, Moore AM, Babb K, Fried MG, Stevenson B. 2010. BpaB, a novel
692 protein encoded by the Lyme disease spirochete's cp32 prophages, binds to *erp* Operator
693 2 DNA. Nucleic Acids Res 38:5443-55.

694 56. Jutras BL, Verma A, Adams CA, Brissette CA, Burns LH, Whetstine CR, Bowman A,
695 Chenail AM, Zuckert WR, Stevenson B. 2012. BpaB and EbfC DNA-binding proteins
696 regulate production of the Lyme disease spirochete's infection-associated Erp surface
697 proteins. J Bacteriol 194:778-86.
698 57. Jutras BL, Chenail AM, Carroll DW, Miller MC, Zhu H, Bowman A, Stevenson B. 2013.
699 Bpur, the Lyme disease spirochete's PUR domain protein: identification as a
700 transcriptional modulator and characterization of nucleic acid interactions. J Biol Chem
701 288:26220-34.
702 58. Si F, Li D, Cox SE, Sauls JT, Azizi O, Sou C, Schwartz AB, Erickstad MJ, Jun Y, Li X,
703 Jun S. 2017. Invariance of Initiation Mass and Predictability of Cell Size in *Escherichia*
704 *coli*. Curr Biol 27:1278-1287.
705 59. Myrbraten IS, Wiull K, Salehian Z, Havarstein LS, Straume D, Mathiesen G, Kjos M.
706 2019. CRISPR Interference for Rapid Knockdown of Essential Cell Cycle Genes in
707 *Lactobacillus plantarum*. mSphere 4.
708 60. Bjånes E, Stream A, Gibson PS, Bravo AM, Dahesh S, Baker JL, Varble A, Nizet V,
709 Veening J-W. 2024. An efficient *in vivo*-inducible CRISPR interference system for group
710 A *Streptococcus* genetic analysis and pathogenesis studies. bioRxiv
711 doi:10.1101/2024.02.22.581527:2024.02.22.581527.
712 61. Fenster JA, Werner AZ, Tay JW, Gillen M, Schirokauer L, Hill NC, Watson A, Ramirez
713 KJ, Johnson CW, Beckham GT, Cameron JC, Eckert CA. 2022. Dynamic and single cell
714 characterization of a CRISPR-interference toolset in *Pseudomonas putida* KT2440 for β-
715 ketoadipate production from p-coumarate. Metab Eng Commun 15:e00204.

716 62. Meunier A, Cornet F, Campos M. 2021. Bacterial cell proliferation: from molecules to
717 cells. FEMS Microbiol Rev 45.
718 63. Jutras BL, Scott M, Parry B, Biboy J, Gray J, Vollmer W, Jacobs-Wagner C. 2016. Lyme
719 disease and relapsing fever *Borrelia* elongate through zones of peptidoglycan synthesis
720 that mark division sites of daughter cells. Proc Natl Acad Sci U S A 113:9162-70.
721 64. Van De Putte P, Van D, Roersch A. 1964. The selection of mutants of *Escherichia coli*
722 with impaired cells division at elevated temperature. Mutat Res 106:121-8.
723 65. Wang H, Henk MC, Gayda RC. 1993. Overexpression of *ftsA* induces large bulges at the
724 septal regions in *Escherichia coli*. Current Microbiology 26:175-181.
725 66. Meisner J, Montero Llopis P, Sham LT, Garner E, Bernhardt TG, Rudner DZ. 2013.
726 FtsEX is required for CwlO peptidoglycan hydrolase activity during cell wall elongation
727 in *Bacillus subtilis*. Mol Microbiol 89:1069-83.
728 67. Li J, Xu X, Shi J, Hermoso JA, Sham L-T, Luo M. 2023. Regulation of the cell division
729 hydrolase RipC by the FtsEX system in *Mycobacterium tuberculosis*. Nature
730 Communications 14:7999.
731 68. Xu X, Li J, Chua W-Z, Pages MA, Shi J, Hermoso JA, Bernhardt T, Sham L-T, Luo M.
732 2023. Mechanistic insights into the regulation of cell wall hydrolysis by FtsEX and EnvC
733 at the bacterial division site. Proceedings of the National Academy of Sciences
734 120:e2301897120.
735 69. Du S, Pichoff S, Lutkenhaus J. 2016. FtsEX acts on FtsA to regulate divisome assembly
736 and activity. Proceedings of the National Academy of Sciences 113:E5052-E5061.

70. Diez AA, Farewell A, Nannmark U, Nyström T. 1997. A mutation in the *ftsK* gene of *Escherichia coli* affects cell-cell separation, stationary-phase survival, stress adaptation, and expression of the gene encoding the stress protein UspA. J Bacteriol 179:5878-83.

71. Liu G, Draper GC, Donachie WD. 1998. FtsK is a bifunctional protein involved in cell division and chromosome localization in *Escherichia coli*. Mol Microbiol 29:893-903.

72. Steiner W, Liu G, Donachie WD, Kuempel P. 1999. The cytoplasmic domain of FtsK protein is required for resolution of chromosome dimers. Mol Microbiol 31:579-83.

73. Crozat E, Rousseau P, Fournes F, Cornet F. 2014. The FtsK family of DNA translocases finds the ends of circles. J Mol Microbiol Biotechnol 24:396-408.

74. Yu XC, Weihe EK, Margolin W. 1998. Role of the C terminus of FtsK in *Escherichia coli* chromosome segregation. J Bacteriol 180:6424-8.

75. Capiaux H, Lesterlin C, Pérals K, Louarn JM, Cornet F. 2002. A dual role for the FtsK protein in *Escherichia coli* chromosome segregation. EMBO Rep 3:532-6.

76. Aussel L, Barre FX, Aroyo M, Stasiak A, Stasiak AZ, Sherratt D. 2002. FtsK Is a DNA motor protein that activates chromosome dimer resolution by switching the catalytic state of the XerC and XerD recombinases. Cell 108:195-205.

77. Begg KJ, Dewar SJ, Donachie WD. 1995. A new *Escherichia coli* cell division gene, *ftsK*. J Bacteriol 177:6211-22.

78. Grenga L, Luzi G, Paolozzi L, Ghelardini P. 2008. The *Escherichia coli* FtsK functional domains involved in its interaction with its divisome protein partners. FEMS microbiology letters 287:163-167.

758 79. Chen JC, Beckwith J. 2001. FtsQ, FtsL and FtsI require FtsK, but not FtsN, for co-
759 localization with FtsZ during *Escherichia coli* cell division. Molecular microbiology
760 42:395-413.
761 80. Sperandio V, Torres AG, Kaper JB. 2002. Quorum sensing *Escherichia coli* regulators B
762 and C (QseBC): a novel two-component regulatory system involved in the regulation of
763 flagella and motility by quorum sensing in *E. coli*. Mol Microbiol 43:809-21.
764 81. Savage CR, Jutras BL, Bestor A, Tilly K, Rosa PA, Tourand Y, Stewart PE, Brissette
765 CA, Stevenson B. 2018. *Borrelia burgdorferi* SpoVG DNA- and RNA-Binding Protein
766 Modulates the Physiology of the Lyme Disease Spirochete. J Bacteriol 200.
767 82. Saylor TC, Savage CR, Krusenstjerna AC, Jusufovic N, Zuckert WR, Brissette CA,
768 Motaleb M, Schlax PJ, Stevenson B. 2023. Quantitative analyses of interactions between
769 SpoVG and RNA/DNA. Biochem Biophys Res Commun 654:40-46.
770 83. Pappas CJ, Iyer R, Petzke MM, Caimano MJ, Radolf JD, Schwartz I. 2011. *Borrelia*
771 *burgdorferi* requires glycerol for maximum fitness during the tick phase of the enzootic
772 cycle. PLoS Pathog 7:e1002102.
773 84. He M, Ouyang Z, Troxell B, Xu H, Moh A, Piesman J, Norgard MV, Gomelsky M, Yang
774 XF. 2011. Cyclic di-GMP is essential for the survival of the Lyme disease spirochete in
775 ticks. PLoS pathogens 7:e1002133.
776 85. Caimano MJ, Dunham-Ems S, Allard AM, Cassera MB, Kenedy M, Radolf JD. 2015.
777 Cyclic di-GMP modulates gene expression in Lyme disease spirochetes at the tick-
778 mammal interface to promote spirochete survival during the blood meal and tick-to-
779 mammal transmission. Infect Immun 83:3043-60.

86. Blevins JS, Xu H, He M, Norgard MV, Reitzer L, Yang XF. 2009. Rrp2, a sigma54-dependent transcriptional activator of *Borrelia burgdorferi*, activates *rpoS* in an enhancer-independent manner. J Bacteriol 191:2902-5.

87. Xu Q, Shi Y, Dadhwal P, Liang FT. 2012. RpoS regulates essential virulence factors remaining to be identified in Borrelia burgdorferi. PLoS One 7:e53212.

88. Ouyang Z, Zhou J, Norgard MV. 2014. Synthesis of RpoS is dependent on a putative enhancer binding protein Rrp2 in *Borrelia burgdorferi*. PLoS One 9:e96917.

89. Samuels DS. 2011. Gene regulation in *Borrelia burgdorferi*. Annual review of microbiology 65:479-99.

90. Castro-Padovani TN, Saylor TC, Husted OT, Krusenstjerna AC, Jusufovic N, Stevenson B. 2023. Gac Is a Transcriptional Repressor of the Lyme Disease Spirochete's OspC Virulence-Associated Surface Protein. J Bacteriol doi:10.1128/jb.00440-22:e0044022.

91. Rollend L, Fish D, Childs JE. 2013. Transovarial transmission of *Borrelia* spirochetes by *Ixodes scapularis*: a summary of the literature and recent observations. Ticks Tick Borne Dis 4:46-51.

92. Casjens S, van Vugt R, Tilly K, Rosa PA, Stevenson B. 1997. Homology throughout the multiple 32-kilobase circular plasmids present in Lyme disease spirochetes. J Bacteriol 179:217-27.

93. Barbour AG, Hayes SF, Heiland RA, Schrumpf ME, Tessier SL. 1986. A *Borrelia*-specific monoclonal antibody binds to a flagellar epitope. Infect Immun 52:549-54.

94. El-Hage N, Babb K, Carroll JA, Lindstrom N, Fischer ER, Miller JC, Gilmore RD, Jr., Mbow ML, Stevenson B. 2001. Surface exposure and protease insensitivity of *Borrelia burgdorferi* Erp (OspEF-related) lipoproteins. Microbiology (Reading) 147:821-830.

803 95. Song X, Goedhart J. 2024. EzReverse – a Web Application for Background Adjustment
804 of Color Images. bioRxiv doi:10.1101/2024.05.27.594095:2024.05.27.594095.
805 96. Goedhart J, Luijsterburg MS. 2020. VolcaNoseR is a web app for creating, exploring,
806 labeling and sharing volcano plots. Scientific Reports 10.
807 97. Kolde R, Kolde MR. 2015. Package 'pheatmap'. R package 1:790.
808 98. Zhao X, Zhang K, Boquoi T, Hu B, Motaleb MA, Miller KA, James ME, Charon NW,
809 Manson MD, Norris SJ, Li C, Liu J. 2013. Cryoelectron tomography reveals the
810 sequential assembly of bacterial flagella in *Borrelia burgdorferi*. Proc Natl Acad Sci U S
811 A 110:14390-5.
812 99. Qin Z, Tu J, Lin T, Norris SJ, Li C, Motaleb MA, Liu J. 2018. Cryo-electron tomography
813 of periplasmic flagella in *Borrelia burgdorferi* reveals a distinct cytoplasmic ATPase
814 complex. PLoS Biol 16:e3000050.
815 100. Chang Y, Moon KH, Zhao X, Norris SJ, Motaleb MA, Liu J. 2019. Structural insights
816 into flagellar stator–rotor interactions. eLife 8:e48979.
817

818 # Figure Legends.

819 **Figure 1. Validation of conditional dysregulation of DnaA. (A)** Two sgRNAs were designed
820 to knock down borrelial *dnaA* transcription by CRISPRi. One sgRNA targeted the template
821 strand directly upstream of the ORF ($dnaA_{T1}$), while the other targeted the template strand within
822 the ORF ($dnaA_{NT1}$). **(B)** The *dnaA* CRISPRi bacteria, CRISPRi empty vector bacteria, and the
823 strain with the *dnaA* overexpression plasmid grew at the same rate as the parental e2. Adding
824 IPTG to these strains resulted in appropriate knockdown or overexpression of DnaA protein **(C)**
825 and transcript **(D)**, as assessed by immunoblot and qRT-PCR. The overexpression shuttle vector
826 encodes a DnaA with an N-terminal 3xFLAG moiety and thus migrates above the native protein.
827 Error bars in (B) and (D) represent the standard error of the mean (SEM).
828
829 **Figure 2. Appropriate expression of DnaA is required for *B. burgdorferi* replication. (A)**
830 Growth curve studies were conducted on different *B. burgdorferi* strains incubated with 0.5 mM
831 IPTG. Three independent cultures of each strain were measured for growth curve analysis. Error
832 bars represent the SEM. The dashed line indicates when the overexpression strain resumed
833 growth. **(B)** The generation time was determined from the growth curve analyses from three
834 individual cultures of each strain. For the overexpression strain, the growth rate was determined
835 before (early; 1-4 dpi) and after the resumption of growth (late; 4-7 dpi). The resumption of
836 replication in that strain was evidently due to mutation of the overexpressed *dnaA* gene. The p-
837 values are indicated as follows: **, $p \leq 0.01$; ***, $p \leq 0.001$; ns, not significant, $p > 0.05$. **(C)**
838 IPTG-treated DnaA overexpression spirochetes that resumed growth (conditioned) lost
839 sensitivity to IPTG when passaged to fresh media and did not overproduce 3xFLAG-DnaA as
840 assessed by immunoblot **(D)**, supporting the conclusion that accumulated mutations in the

overexpression *dnaA* permitted replication. **(E)** Sequenced plasmid from these conditioned spirochetes showed unique mutations (S = substitution; I= Insertion; D = deletion) in the 3xFLAG-*dnaA* ORF that caused a frameshift and truncation of the full-length protein. The location of the truncation is indicated by *.

Figure 3. DnaA dysregulation affects spirochete cell length. (A-D) Cell lengths of the 0.5 mM IPTG-treated *B. burgdorferi* B31-e2 strains measured over seven days (gray = e2; red = $dnaA_{T1}$; $dnaA_{NT1}$ = blue; P_{lac}::3xFLAG-*dnaA* = purple). The line represents the median cell length. **(E-H)** The median cell length (filled-in circle) with error bars representing the 95% CI superimposed against the corresponding growth curve (empty circle) from Fig. 2. The dashed line indicates when the overexpression strain resumed growth. **(I-K)** Representative images of observed phenotypes. **(I)** The e2 cell of approximate median length at 2 dpi. **(J)** DnaA-depleted cell with the characteristic elongation phenotype. **(K)** Median size of a DnaA overexpression spirochete at 2 dpi.

Figure 4. Knockdown of DnaA increases the number of chromosomes per spirochete. The *B. burgdorferi* CRISPRi $dnaA_{T1}$ and parent B31-e2 strains were transformed with a construct encoding a mCherry-tagged ParB protein, which binds near the *oriC*, to identify the locations of the chromosomes. The two strains were grown without inducer until mid-log (t = 0), and then the $dnaA_{T1}$ strain was divided into two cultures, and one of those was induced with 0.5 mM IPTG. Cultures were tracked for three more days. **(A)** Representative merged micrographs (blue = dark field; red = mCherry-ParB) of spirochetes with the approximate median numbers of ParB-*oriC* puncta **(B)** and cell length **(C)**. Significant differences in numbers of puncta and cell length at day 0 were determined by the Mann-Whitney U test. Differences between the three groups (e2, -

IPTG, and + IPTG) on days 1-3 were tested for by the Kruskal-Wallis test and then Dunn's test for multiple comparisons. Multiplicity-adjusted p-values are reported. **, $p \leq 0.01$; ***, $p \leq 0.001$; ****, $p \leq 0.0001$; ns, not significant, $p > 0.05$. Approximately 50 spirochetes were imaged for each strain on each day. Data were gathered from two independent experiments.

Figure 5. Irregular spacing of *oriC* in *dnaA* knockdown *B. burgdorferi*. (A-B) Representative images of spirochetes containing the *dnaA*$_{T1}$ CRISPRi plasmid with irregular spacing of ParB-*oriC* puncta (red). DnaA-depleted cells had large regions where no foci were observed (brackets). Some cells also had foci that were close together (arrows). **(C)** Parental B31-e2 spirochetes with approximately the same number of ParB-*oriC* puncta as the mutant but exhibit regular oriC spacing. **(D)** The number of spirochetes with irregular ParB-*oriC* was quantified (e2, $n = 184$; uninduced *dnaA*$_{T1}$, $n = 198$ cells; induced *dnaA*$_{T1}$ $n = 206$). One-way ANOVA with Tukey's post-hoc test was done to determine the significance and make comparisons. The multiplicity-adjusted p-values are reported **, $p \leq 0.01$; ns, not significant, $p > 0.05$.

Figure 6. DnaA-depletion affects borrelial helicity. Representative micrographs of observed phenotypes. When *dnaA* was knocked down, spirochetes with no **(A)** or asymmetrical helicity **(B)** were observed. **(C)** Some of the abnormal cells were elongated and showed division defects. **(D)** Spirochetes exhibiting similar defects were observed at a low level in the B31-e2 strain (0.7%, $n = 1514$). The empty vector (EV) control cultures had a similar proportion, independent of the addition of IPTG (uninduced: 2.1%, $n = 1439$; induced: 1.6%, $n = 1608$). The bacteria with the *dnaA*$_{T1}$ CRISPRi plasmid had significantly more cells with perturbed helicity that was dependent on induction (uninduced: 8.7%, $n = 1437$; induced: 13%, $n = 1472$). Spirochetes were

888 counted from three independent cultures. Statistical significance was determined by one-way
889 ANOVA with a Holm-Šídák's post-hoc test, and multiplicity-adjusted p-values are reported. ***,
890 $p \leq 0.001$, ****, $p \leq 0.0001$; ns, not significant, $p > 0.05$.
891
892 **Figure 7. RNA-seq of DnaA-dysregulated *B. burgdorferi*.** The RNA from three *B. burgdorferi*
893 strains with different cellular levels of DnaA were sequenced: B31-e2 (parent), CRISPRi $dnaA_{T1}$
894 (DnaA-down), and overexpression pACK121 (DnaA-up). **(A-C)** Volcano plots plotting the fold
895 change ($\log_2$FC) against each gene's false discovery rate ($-\log_{10}$(FDR)). The threshold for
896 significance was set at a $\log_2$FC ≥ 1 or ≤ -1 ($\geq$ 2-fold change) and an FDR of ≤ 0.05. **(D)** PCA
897 plot showing the clustering of the replicate samples that were sequenced. **(E)** Donut charts
898 showing the replicons on which the significantly affected genes are encoded. **(F)** qRT-PCR
899 results of *dnaA* transcripts in the sequenced samples. Cq values were normalized to *ftsK* or *rpoB*
900 (ΔCq) and then to the parental strain (ΔΔCq). Error bars represent the standard deviation (SD).
901
902 **Figure 8. Impacts of DnaA on *B. burgdorferi* elongation and division genes. (A)** Heat map of
903 the division and elongation genes that were significantly affected when DnaA was knocked
904 down. **(B)** Top: Locus maps of the select elongation and division genes to scale. The sites of
905 potential DnaA-boxes are denoted as purple boxes below the genes. Bottom: Simplified schema
906 of the hypothesized borrelial elongasome and divisome containing the highlighted genes of
907 interest. Informed by the work of Liu et al. and Hu et al. (36, 69) **(C)** Bar graph showing the fold
908 change detected by RNA-seq of the elongation and division genes. The dashed lines indicate the
909 2-fold threshold for meaningful gene expression changes.
910

Figure 9. Impacts of DnaA on *B. burgdorferi* flagellar genes. (A) The borrelial flagellar motor is a complex molecular machine (bottom right) that is comprised of nearly three dozen proteins encoded in four separate loci on the chromosome (top). The schematic of the *B. burgdorferi* flagellar motor was informed from data by Zhao et al., Qin et al., and Chang et al. (98-100). **(B)** RNA-seq showed the transcripts for five flagellar genes increased when DnaA was knocked down. Two of these genes, FliQ and FliR (purple), are constituents of the flagellar export apparatus. The dashed lines indicate the 2-fold threshold for meaningful gene expression changes.

Figure. 10. Impacts of DnaA on the Erp regulatory network. (A) Solid black lines indicate established interactions. Dashed lines indicate hypothesized interactions. Activation is denoted by lines with arrowheads, and inhibition by lines without arrowheads. Note that co-repressive or anti-repressive activities, i.e., BpuR and EbfC, respectively, are indicated by arrows directed at lines. **(B)** Representative immunoblots from samples of *B. burgdorferi* that were analyzed by RNA-seq. Quantitation of target proteins when DnaA was knocked down **(C)** or overexpressed **(D)**. Band intensities for each replicate immunoblot were normalized to FlaB and then the parental e2 strain. **(C-D)** The dotted lines at 1 represent where the protein abundance is the same as e2. Bar graphs showing the fold change detected by RNA-seq in the DnaA-down/e2 **(E)** and DnaA-up comparisons **(F)**. **(E-F)** The dotted lines indicate the 2-fold threshold for meaningful gene expression changes.

Figure 11. Roles and impacts of DnaA dysregulation on borrelial physiology. The DnaA of *B. burgdorferi* functions as the chromosome replication initiator and a transcription factor.

Altering levels of this essential protein modulate aspects of DNA replication and bacterial physiology. The data presented here point to crosstalk between the systems controlling replication and bacterial morphology. Future studies will need to be conducted to ascertain the direct roles DnaA plays in maintaining this delicate balance.

940 **Table 1.** Homologous elongation and division genes of *B. burgdorferi*.

				RNA-seq Differential Expression		
Protein	**Locus Tag**	**Elongasome**	**Divisome**	**DnaA-down vs e2**	**DnaA-up vs e2**	**DnaA-down vs DnaA-up**
FtsE	BB_0080	-	+	Down	NA	Down
FtsX	BB_0081	-	+	Up	NA	Up
FtsI/PBP3	BB_0136	+	+	NA	NA	NA
MurE	BB_0201	+	+	NA	NA	NA
FtsK	BB_0257	-	+	Down	NA	Down
FtsZ	BB_0299	-	+	NA	NA	NA
FtsA	BB_0300	-	+	Up	Up	NA
FtsQ/DivlB	BB_0301	-	+	NA	NA	NA
FtsW	BB_0302	-	+	NA	NA	NA
MraY	BB_0303	+	+	NA	NA	NA
MurF	BB_0304	+	+	NA	NA	NA
MurD	BB_0585	+	+	NA	NA	NA
MurB	BB_0598	+	+	NA	NA	NA
Ami	BB_0666	-	+	NA	NA	NA
MreB	BB_0715	+	-	Down	NA	Down
MreC	BB_0716	+	-	Down	NA	Down
MreD	BB_0717	+	-	Up	NA	Up
PBP2	BB_0718	+	-	Down	NA	Down
RodA	BB_0719	+	-	NA	NA	NA
PBP1a	BB_0732	+	-	Down	NA	Down
MurG	BB_0767	+	+	NA	NA	NA
MurJ	BB_0810	+	+	NA	Down	Up
MurC	BB_0817	+	+	NA	NA	NA

941 * Plus sign (+) indicates the protein is part of the complex, minus sign (-) indicates it is not

942 * NA = Not affected

943

944 **Table 2.** Oligonucleotides used in this study.

Target	Name	Sequence	Purpose	Source
dnaA ORF	qPCR *dnaA* F	CATGTGACCGATCTCCTTCTG	qPCR	(10)
	qPCR *dnaA* R	CGACAATAGCTGCTCTGAGTT		
ftsK ORF	qPCR *ftsK* F	GACCTTCTGATGAGCCAATGT	qPCR	(10)
	qPCR *ftsk* R	GCTGCTCTGTTGTAACCTATCT		
rpoB ORF	qPCR *rpoB* F	GTTCATCTGGGACAAGGAAGAG	qPCR	This study
	qPCR *rpoB* R	CAGACTCAAGGCCCTCATTAAG		

945

Figure 1.

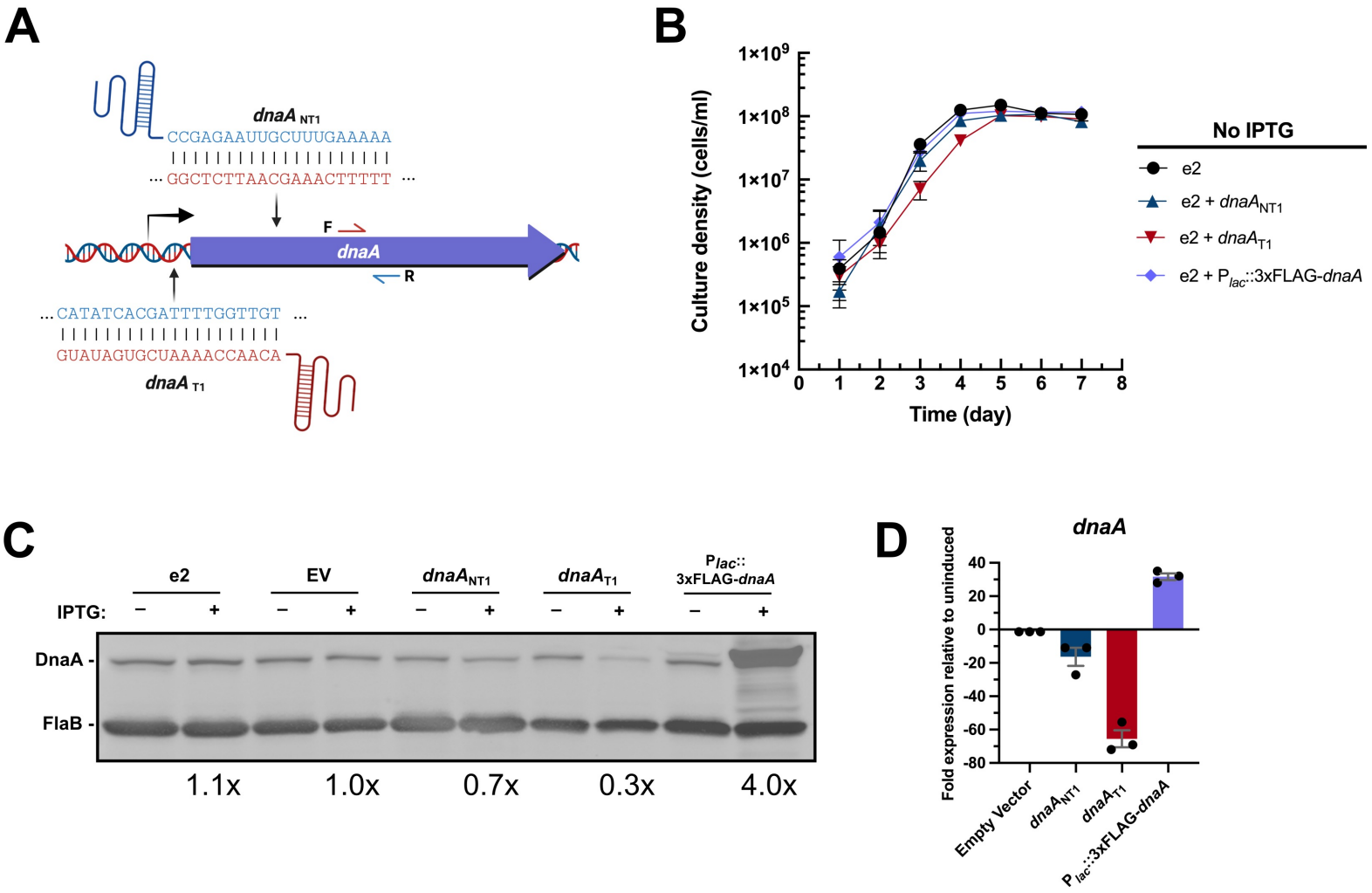
A
dnaA NT1
CCGAGAAUUGCUUUGAAAAA
GGCTCTTAACGAAACTTTTT
F
dnaA
R
CATATCACGATTTTGGTTGT
GUAUAGUGCUAAAACCAACA
dnaA T1
B
Culture density (cells/ml)
1×10^9
1×10^8
1×10^7
1×10^6
1×10^5
1×10^4
0 1 2 3 4 5 6 7 8
Time (day)
No IPTG
e2
e2 + dnaA_NT1
e2 + dnaA_T1
e2 + P_lac::3xFLAG-dnaA
C
e2
EV
dnaA_NT1
dnaA_T1
P_lac:: 3xFLAG-dnaA
IPTG: – + – + – + – + – +
DnaA
FlaB
1.1x 1.0x 0.7x 0.3x 4.0x
D
dnaA
Fold expression relative to uninduced
40 20 0 -20 -40 -60 -80
Empty Vector
dnaA_NT1
dnaA_T1
P_lac::3xFLAG-dnaA

Figure 2.

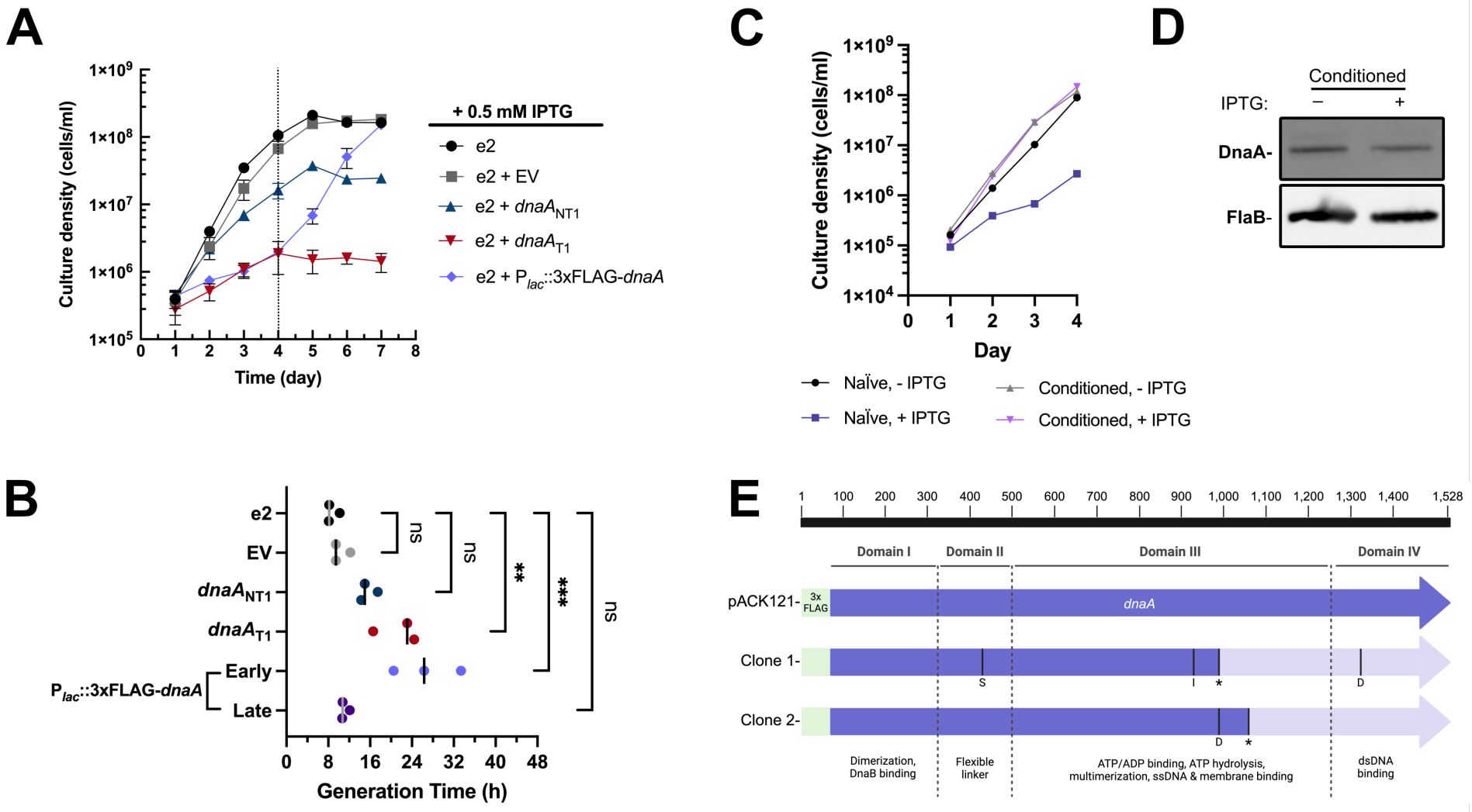
A
Culture density (cells/ml)
Time (day)
+ 0.5 mM IPTG
e2
e2 + EV
e2 + dnaA_NT1
e2 + dnaA_T1
e2 + P_lac::3xFLAG-dnaA
B
e2
EV
dnaA_NT1
dnaA_T1
Early
Late
P_lac::3xFLAG-dnaA
ns
ns
**
***
ns
Generation Time (h)
C
Culture density (cells/ml)
Day
Naïve, - IPTG
Naïve, + IPTG
Conditioned, - IPTG
Conditioned, + IPTG
D
Conditioned
IPTG:
DnaA-
FlaB-
E
Domain I
Domain II
Domain III
Domain IV
pACK121-
3x FLAG
dnaA
Clone 1-
Clone 2-
Dimerization, DnaB binding
Flexible linker
ATP/ADP binding, ATP hydrolysis, multimerization, ssDNA & membrane binding
dsDNA binding

Figure 3.

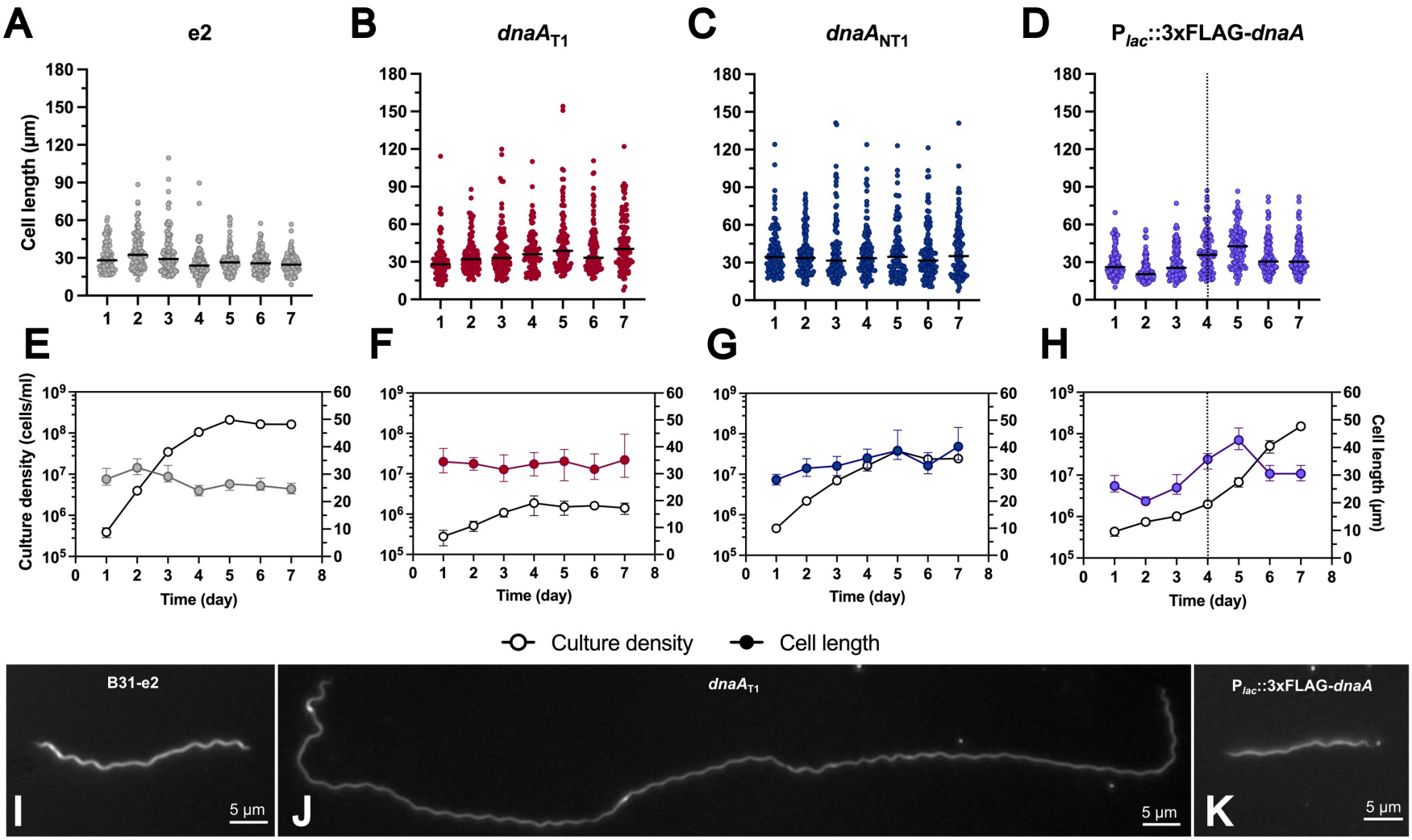
A
e2
B
dnaA_T1
C
dnaA_NT1
D
P_lac::3xFLAG-dnaA
Cell length (μm)
E
F
G
H
Culture density (cells/ml)
Cell length (μm)
Time (day)
Culture density
Cell length
B31-e2
dnaA_T1
P_lac::3xFLAG-dnaA
I
J
K
5 μm

Figure 4.

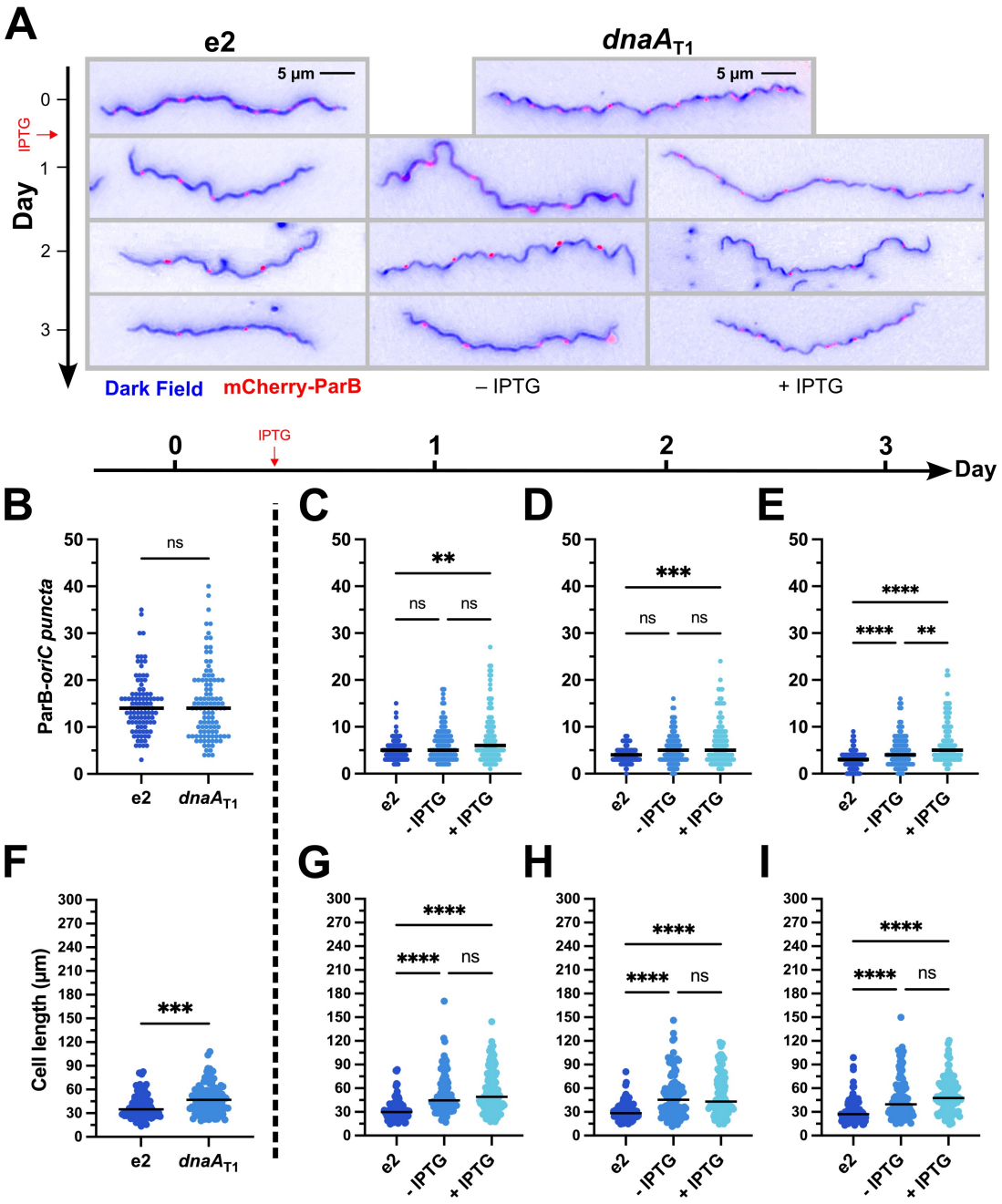
A
e2
dnaA T1
5 µm
5 µm
IPTG
Day
0
1
2
3
Dark Field
mCherry-ParB
– IPTG
+ IPTG
0
IPTG
1
2
3
Day
B
C
D
E
ParB-oriC puncta
ns
**
***
****
e2
dnaA T1
- IPTG
+ IPTG
F
G
H
I
Cell length (µm)
***
****

Figure 5.

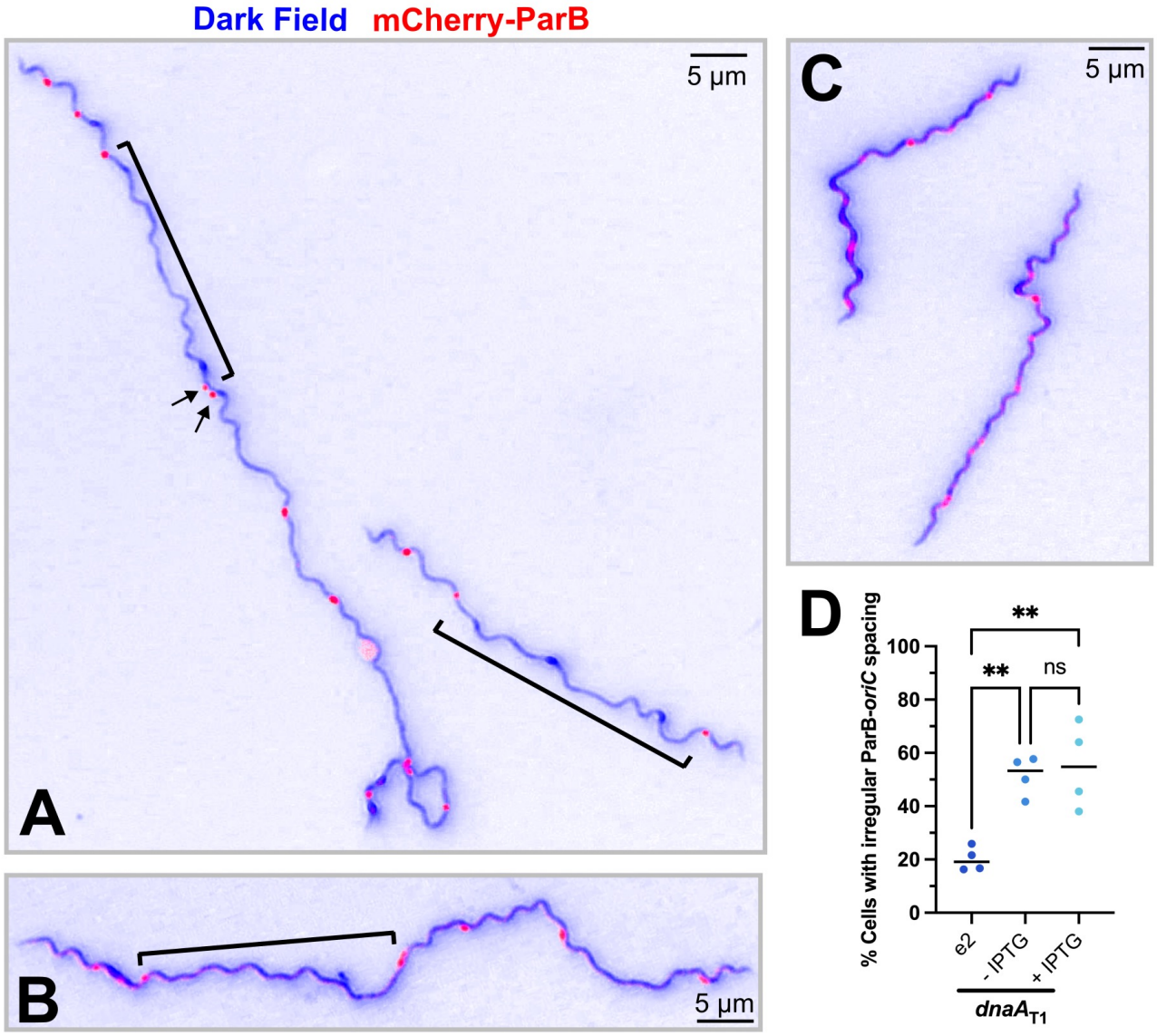
Dark Field
mCherry-ParB
5 µm
A
B
5 µm
C
5 µm
D
% Cells with irregular ParB-oriC spacing
100
80
60
40
20
0
**
**
ns
e2
- IPTG
+ IPTG
dnaA T1

Figure 6.

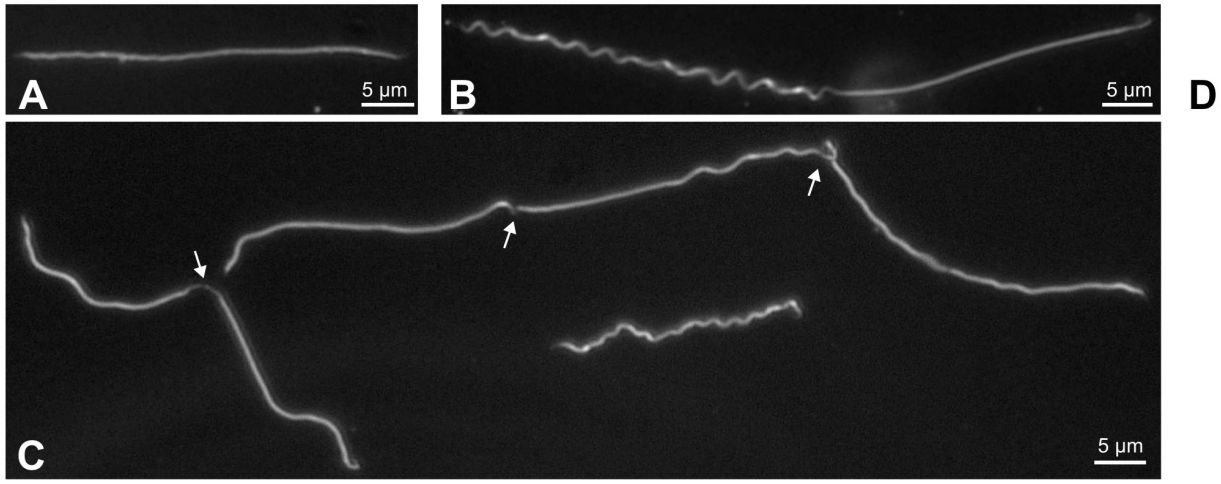
A
5 µm
B
5 µm
C
5 µm

D

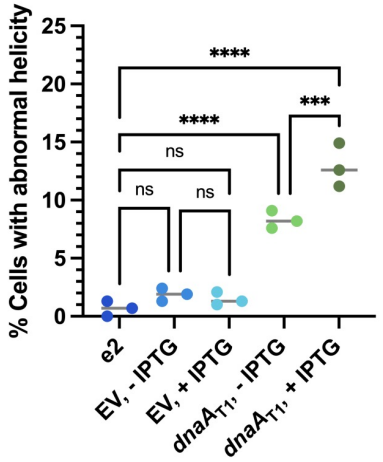
% Cells with abnormal helicity
25
20
15
10
5
0
****
****
***
ns
ns
ns
e2
EV, - IPTG
EV, + IPTG
dnaA$_{T1}$, - IPTG
dnaA$_{T1}$, + IPTG

Figure 7.

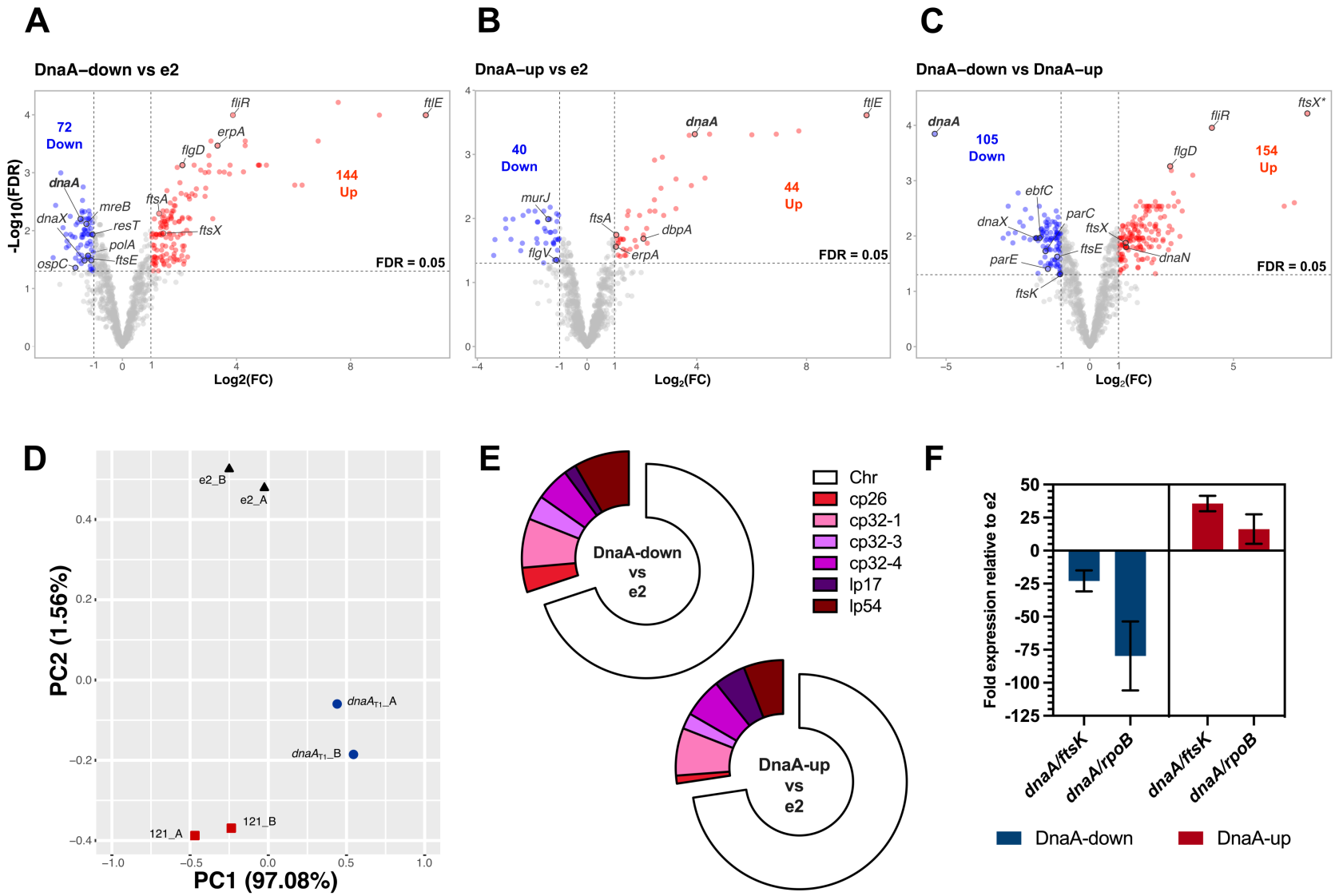
A
DnaA–down vs e2
72
Down
144
Up
FDR = 0.05
-Log10(FDR)
Log2(FC)
fliR
fliE
erpA
flgD
dnaA
mreB
ftsA
dnaX
resT
ftsX
polA
ftsE
ospC
B
DnaA–up vs e2
40
Down
44
Up
FDR = 0.05
Log2(FC)
fliE
dnaA
murJ
ftsA
dbpA
flgV
erpA
C
DnaA–down vs DnaA–up
105
Down
154
Up
FDR = 0.05
Log2(FC)
dnaA
fliR
ftsX*
flgD
ebfC
parC
dnaX
ftsX
ftsE
parE
dnaN
ftsK
D
PC2 (1.56%)
PC1 (97.08%)
e2_B
e2_A
dnaAT1_A
dnaAT1_B
121_A
121_B
E
DnaA-down
vs
e2
DnaA-up
vs
e2
Chr
cp26
cp32-1
cp32-3
cp32-4
lp17
lp54
F
Fold expression relative to e2
dnaA/ftsK
dnaA/rpoB
dnaA/ftsK
dnaA/rpoB
DnaA-down
DnaA-up

Figure 8.

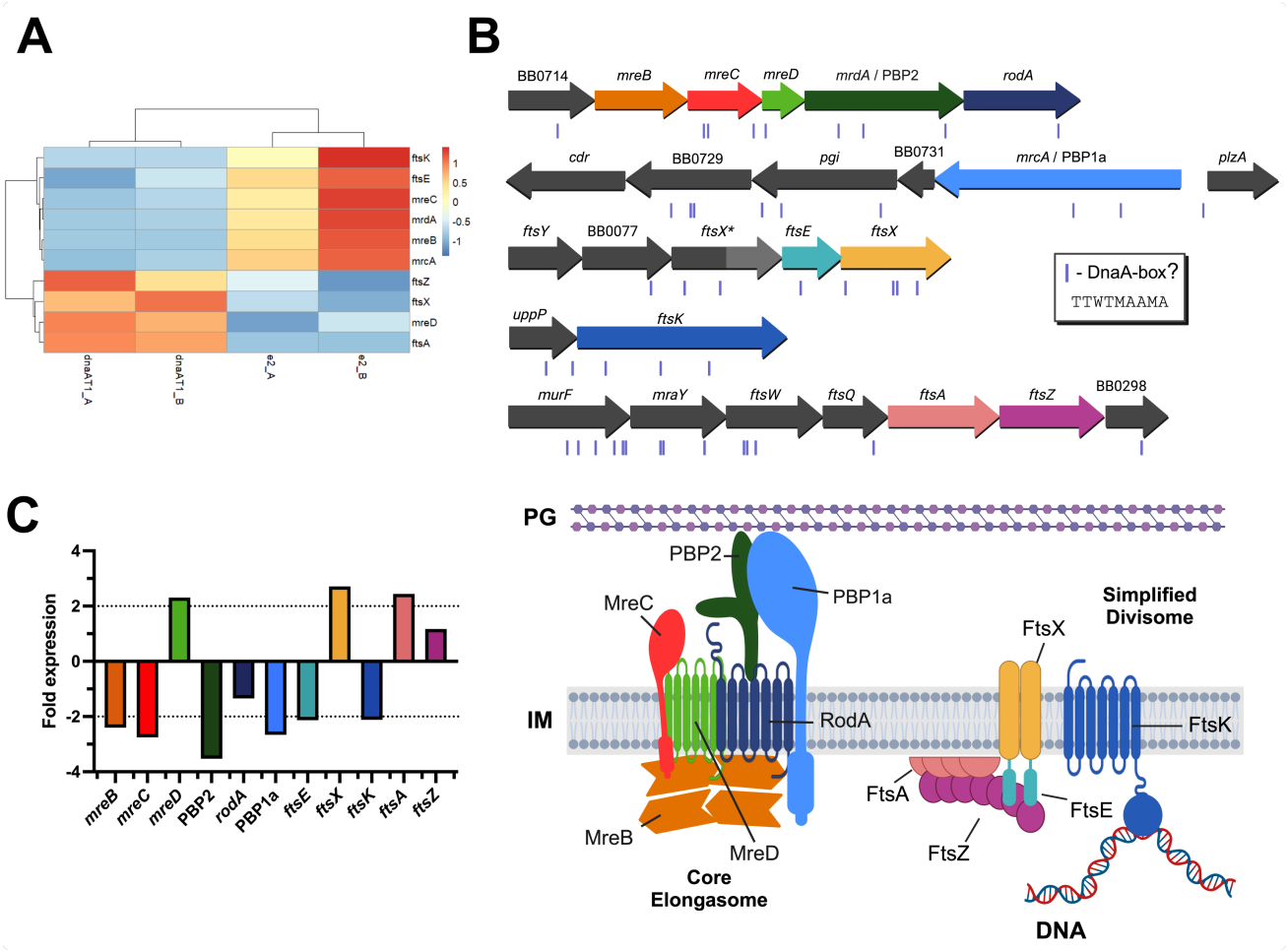
A
ftsK
ftsE
mreC
mrdA
mreB
mrcA
ftsZ
ftsX
mreD
ftsA
1
0.5
0
-0.5
-1
dnaA T1_A
dnaA T1_B
e2_A
e2_B
B
BB0714
mreB
mreC
mreD
mrdA / PBP2
rodA
cdr
BB0729
pgi
BB0731
mrcA / PBP1a
plzA
ftsY
BB0077
ftsX*
ftsE
ftsX
- DnaA-box?
TTWTMAAMA
uppP
ftsK
murF
mraY
ftsW
ftsQ
ftsA
ftsZ
BB0298
C
Fold expression
4
2
0
-2
-4
mreB
mreC
mreD
PBP2
rodA
PBP1a
ftsE
ftsX
ftsK
ftsA
ftsZ
PG
PBP2
PBP1a
MreC
Simplified Divisome
FtsX
IM
RodA
FtsK
FtsA
FtsE
FtsZ
MreB
MreD
Core Elongasome
DNA

Figure 9.

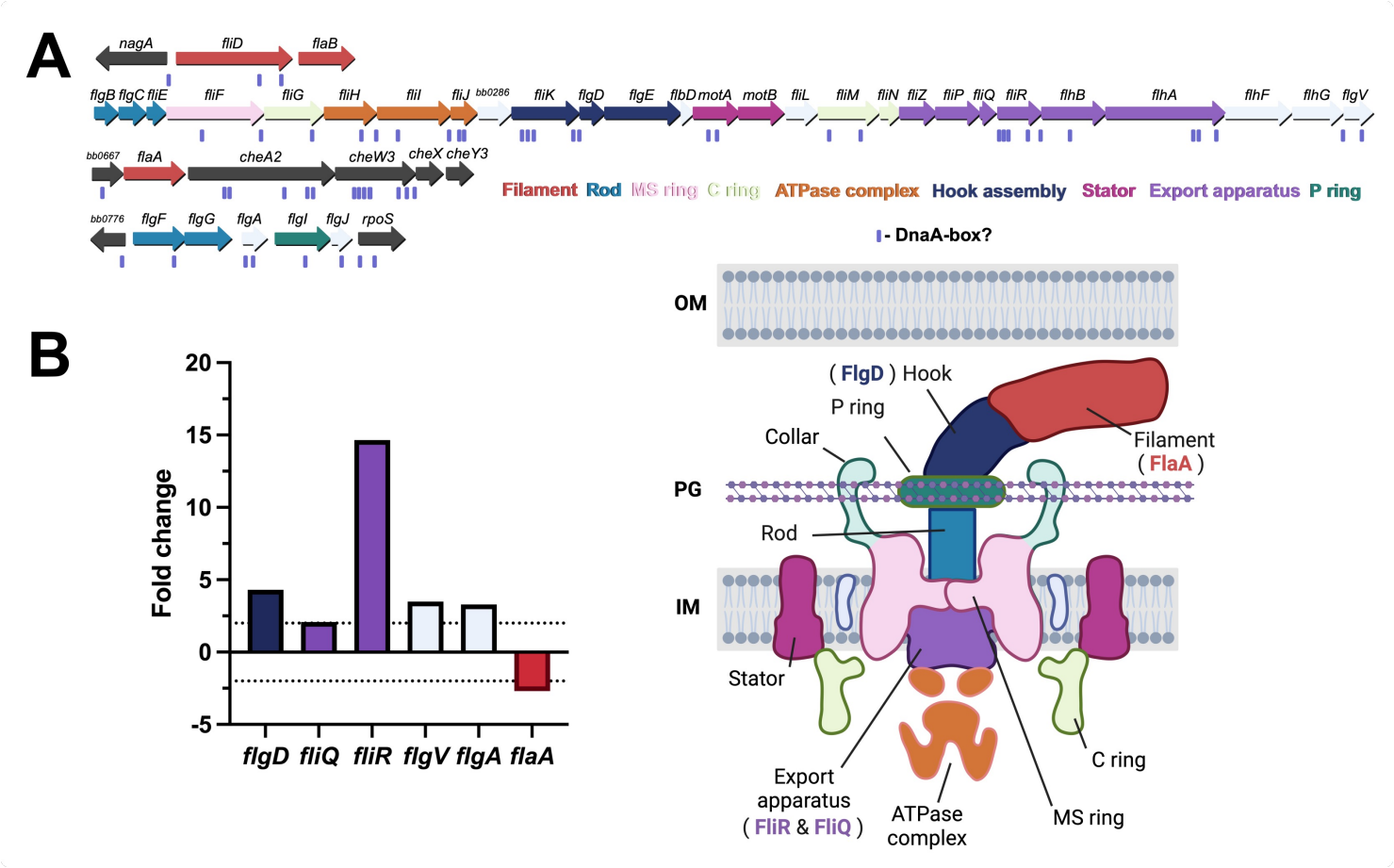
A
nagA fliD flaB
flgB flgC fliE fliF fliG fliH fliI fliJ bb0286 fliK flgD flgE flbD motA motB fliL fliM fliN fliZ fliP fliQ fliR flhB flhA flhF flhG flgV
bb0667 flaA cheA2 cheW3 cheX cheY3
bb0776 flgF flgG flgA flgI flgJ rpoS
Filament Rod MS ring C ring ATPase complex Hook assembly Stator Export apparatus P ring
- DnaA-box?
B
Fold change
20
15
10
5
0
-5
flgD fliQ fliR flgV flgA flaA
OM
PG
IM
(FlgD) Hook
P ring
Collar
Filament
(FlaA)
Rod
Stator
C ring
Export
apparatus
(FliR & FliQ)
ATPase
complex
MS ring

Figure 10.

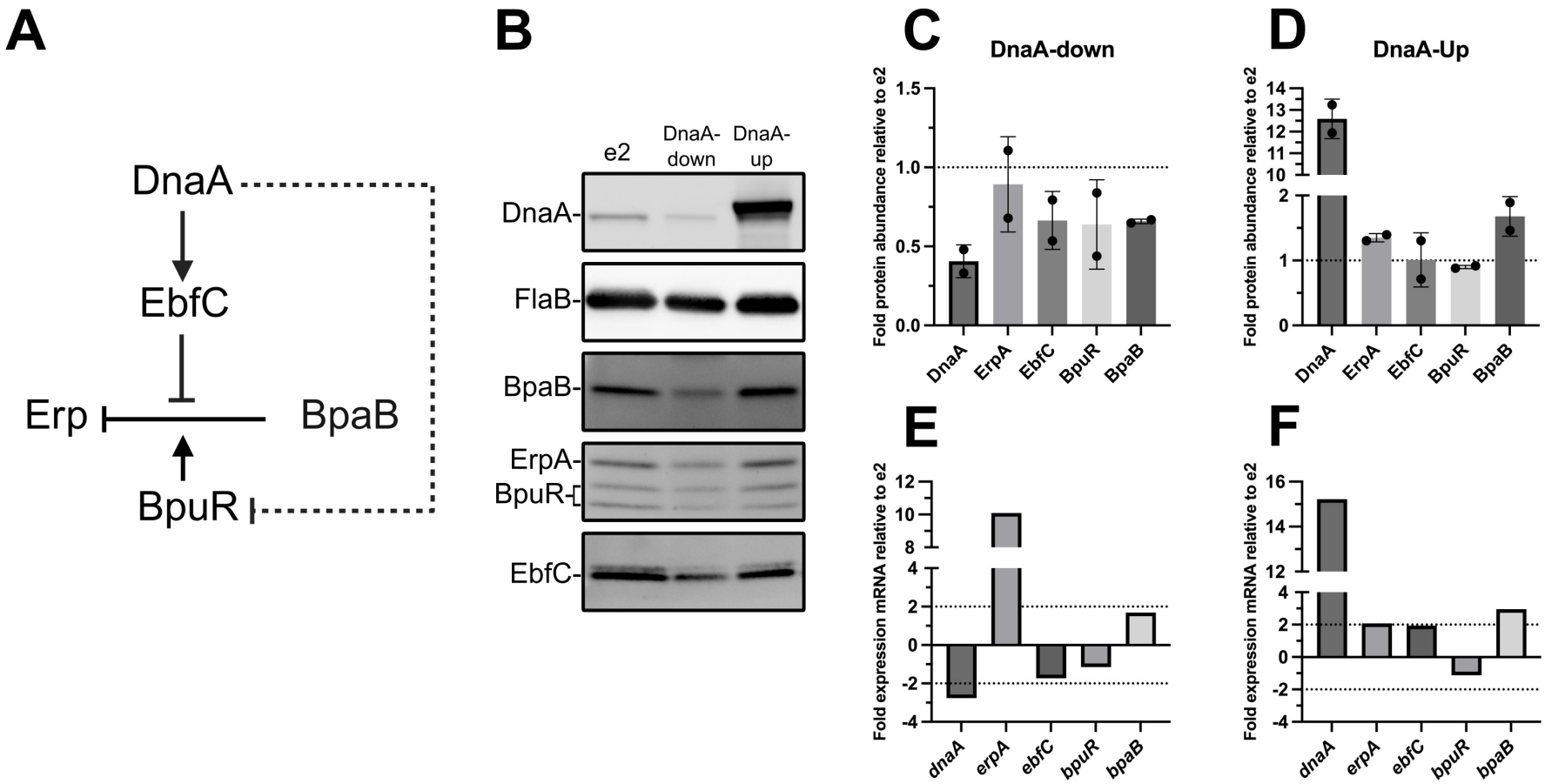
A
DnaA
EbfC
Erp
BpaB
BpuR
B
e2
DnaA-down
DnaA-up
DnaA-
FlaB-
BpaB-
ErpA-
BpuR-
EbfC-
C
DnaA-down
Fold protein abundance relative to e2
1.5
1.0
0.5
0.0
DnaA
ErpA
EbfC
BpuR
BpaB
D
DnaA-Up
Fold protein abundance relative to e2
14
13
12
11
10
2
1
0
DnaA
ErpA
EbfC
BpuR
BpaB
E
Fold expression mRNA relative to e2
12
10
8
4
2
0
-2
-4
dnaA
erpA
ebfC
bpuR
bpaB
F
Fold expression mRNA relative to e2
16
14
12
4
2
0
-2
-4
dnaA
erpA
ebfC
bpuR
bpaB

Figure 11.

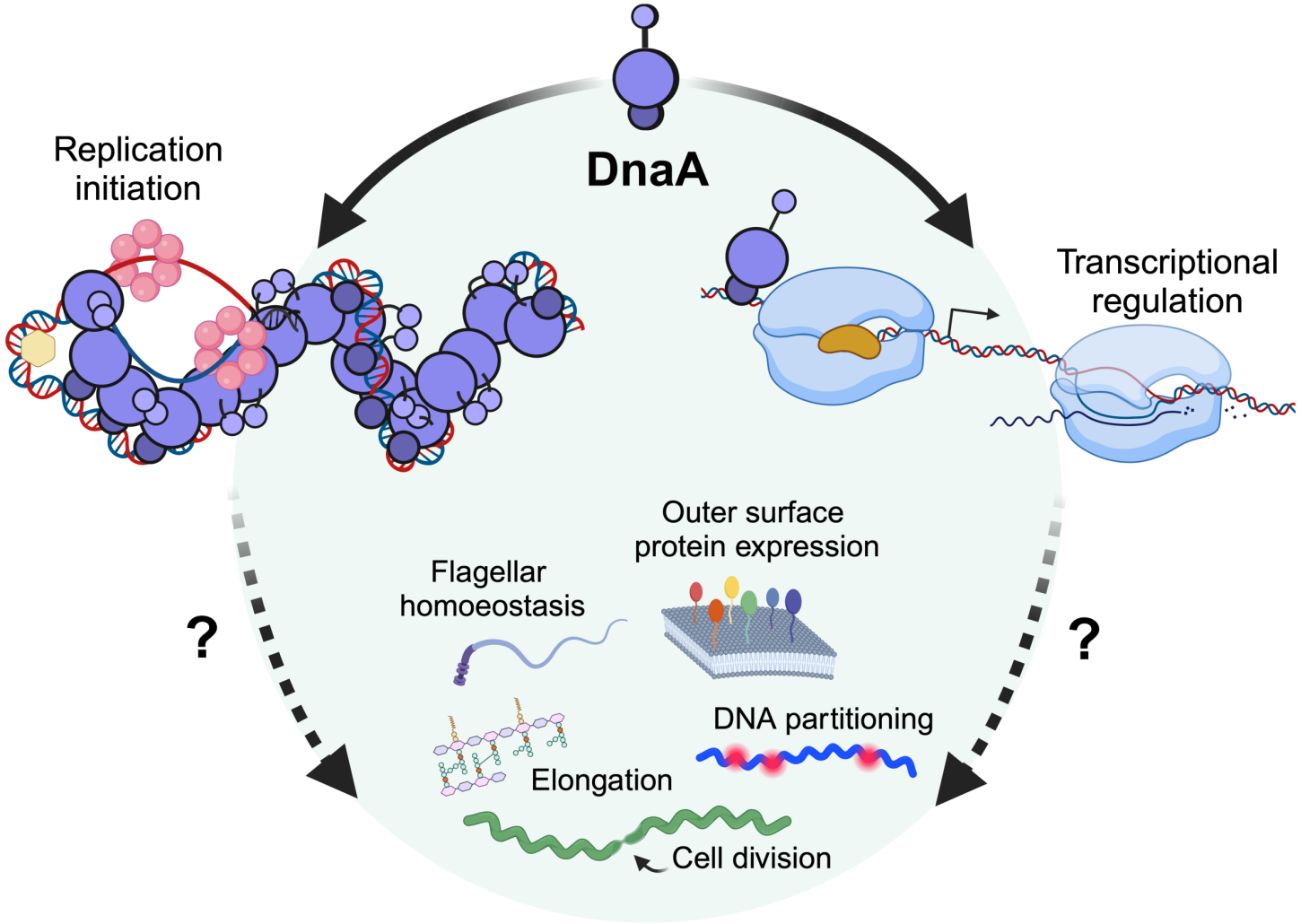
DnaA
Replication initiation
Transcriptional regulation
Outer surface protein expression
Flagellar homoeostasis
DNA partitioning
Elongation
Cell division
?
?